HYBRIDGE

Distributed Control and Stochastic Analysis of Hybrid Systems Supporting Safety Critical Real-Time Systems Design

WP3: Reachability analysis for probabilistic hybrid systems

Reachability Analysis for Probabilistic Hybrid Systems with Application to Air Traffic Management

Maria Prandini[*] and Marco C. Campi[**]

10th November 2004

Version: *1.2*
Task number: *3.1*
Deliverable number: *D3.1*
Contract: *IST-2001-32460 of European Commission*

[*] Politecnico di Milano, Italy
[**] University of Brescia, Italy

DOCUMENT CONTROL SHEET

Title of document: *Reachability Analysis for Probabilistic Hybrid Systems with Application to Air Traffic Management*

Authors of document: *M. Prandini and M.C. Campi*

Deliverable number: *D3.1*

Contract: *IST-2001-32460 of European Commission*

Project: *Distributed Control and Stochastic Analysis of Hybrid Systems Supporting Safety Critical Real-Time Systems Design (HYBRIDGE)*

DOCUMENT CHANGE LOG

Version #	Issue Date	Sections affected	Relevant information
0.1	08/09/2003	All	1st draft
0.2	31/10/2003	All	2nd draft
0.3	30/01/2004	1, 5	Revised based on reviewers' comments
1.0	30/09/2004	1, 2, 3	Revised based on reviewers' comments
1.1	08/10/04	All	Revised based on reviewers' comments
1.2	10/11/04	All	Revised based on reviewers' comments

Version 1.2		Organisation	Signature/Date
Authors	Maria Prandini	UniBs	
	Marco C. Campi	UniBs	
Internal reviewers	Henk Blom	NLR	
	Pascal Lezaud	CENA	
External reviewers	René Boel	Universiteit Gent	
	Jianghai Hu	Purdue University	

HYBRIDGE, IST-2001-32460
Work Package WP3, Deliverable D3.1

Reachability Analysis for Probabilistic Hybrid Systems with Application to Air Traffic Management

Prepared by:
Maria Prandini* and M.C. Campi†

Abstract

This is the first deliverable under workpackage 3 of the HYBRIDGE project, dealing with reachability analysis for air traffic management applications. In general terms, a reachability problem consists of determining if a given system trajectory will eventually enter a pre-specified set starting from some initial state. An important application of reachability analysis is safety verification. In many control applications, the dynamics of the system under study is subjected to the perturbation of random noises that are either inherent or present in the environment. Typically, a certain part of the state space is "unsafe" and the control input to the system has to be chosen so as to keep the state away from it, despite the presence of the random noises. For safety-critical systems operating in a highly dynamic uncertain environment, safety needs to be repeatedly verified on-line based on the updated information on the system behavior, and alarms of different severity can be issued depending on the level of criticality of the situation, according to some structured alerting system. A natural choice for the measure of criticality in this setting is the probability of intrusion into the unsafe set within a finite/infinite time horizon.
In this work we develop a methodology for safety analysis of a certain class of probabilistic hybrid systems, and apply it to probabilistic conflict detection in air traffic management.

*Dipartimento di Elettronica e Informazione, Politecnico di Milano, Piazza Leonardo da Vinci 32, 20133 Milano, Italy, prandini@elet.polimi.it

†Dipartimento di Elettronica per l'Automazione, Università di Brescia, Via Branze 38, 25123 Brescia, Italy, campi@ing.unibs.it

Contents

List of Figures

1 Introduction

This is the first deliverable under workpackage 3 of the HYBRIDGE project and summarizes the achievements of the HYBRIDGE team under Task 3.1 on "Reachability analysis for probabilistic hybrid systems".

The work under Task 3.1 of workpackage 3 was structured in three main streams:

1. review of the methods proposed in the literature for reachability analysis;
2. introduction of a class of probabilistic hybrid systems that are realistic for air traffic management applications but also suitable for theoretical studies;
3. development of a novel reachability analysis approach to probabilistic safety verification for the introduced class of probabilistic hybrid systems, and its application to conflict detection in air traffic management.

1.1 Reachability analysis

In general terms, a reachability problem consists of determining if the trajectories of a given system starting from some set of initial states will eventually enter a pre-specified set.

An important application of reachability analysis is the verification of the correctness of the behavior of a system, which makes reachability analysis relevant in a variety of control applications. In particular, in many safety-critical applications a certain region of the state space is "unsafe", and one has to verify that the system state keeps outside this unsafe set. If the outcome of safety verification is negative, then some action has to be taken to appropriately modify the system.
Given the unsafe set and the set of initial states, a safety verification problem can be reformulated as either a forward reachability problem or a backward reachability problem. Forward reachability consists in determining the set of states that a given system can reach starting from some set of initial states. Conversely, backward reachability consists in determining the set of initial states starting from which the system will eventually enter a given target set of states. One can perform safety verification by showing either that the forward reachable set is disjoint from the unsafe set or that the backward reachable set leading to the unsafe set is disjoint from the set of initial states.

In the model checking approach to safety verification, safety is verified by constructing forward/backward reachable sets based on a model of the system. The main issue of the model checking approach to safety verification is that it requires the ability to "compute" with sets, i.e., to represent sets and propagate them through the system dynamics. This process can be made fully automatic. Model checkers have in fact been developed for different classes of deterministic systems.
In the case of deterministic finite automata, sets can be represented by enumeration, and forward (backward) reachable sets can be computed starting from the given initial (target) set and adding one-step successor (predecessor) till convergence is achieved. Termination of the

algorithm is guaranteed since the state space is finite. Safety verification is then "decidable" for this class of systems, that is, there does exist a computational procedure that decides in a finite number of steps whether safety is verified or not for an arbitrary deterministic finite automata. The technical challenge for the verification of deterministic finite automata is to devise algorithms and data structure to handle large state spaces.
In the case of hybrid systems, two key issues arise due to the uncountable number of states in the continuous state space: i) set representation and propagation by continuous flow is generally difficult; and ii) the state space is not finite, hence termination of the algorithm for reachable set computation is not guaranteed ([1]). Decidability results have been proven for certain classes of hybrid systems by using discrete abstraction consisting in building a finite automaton that is "equivalent" to the original hybrid system for the purpose of safety verification ([2]).
Exact methods for reachability computations exist only for a restricted class of hybrid systems with simple dynamics. In the case of more complex dynamics, approximation methods have been developed, which can be classified as "over-approximation" and "asymptotic approximation" methods.
The over-approximation methods aim at obtaining efficient over-approximations of reachable sets. The main idea is starting from sets that are easy to represent in a compact form and approximating the system dynamics so that the sets obtained through the direct or inverse evolution of the approximated system admit the same representation of the starting sets, while ensuring over-approximation of the reachable sets of the original system. Polyhedral and ellipsoidal methods ([3, 4]) belong to this category of approximation approaches.
The asymptotic approximation methods aim at obtaining an approximation of the reachable sets that converges to the true reachable sets as some accuracy parameter tends to zero. Level set methods and gridding techniques belong to this category. In level set methods, sets are represented as the zero sublevel set of an appropriate function. The evolution of the boundary of this set through the system dynamics can be described through a Hamilton-Jacobi-Isaacs partial differential equation. An approximation to the reachable set is then obtained by a suitable numerical approximation of this equation ([5, 6]). In [7] a Markov chain approximation of a deterministic system is introduced to perform reachability analysis. The Markov chain is obtained by gridding the state space of the original system and defining the transition probabilities over the so-obtained discrete set of states so as to guarantee that admissible trajectories of the original system correspond to trajectories with non zero probability of the Markov chain. If the probability that the Markov chain enters the unsafe set is zero, then, one can conclude that the original system is safe. On the other hand, if such probability is not zero, one cannot conclude that safety is not guaranteed for the original system.
In all approaches, reachability computations become more intensive as the dimension of the continuous state space grows. This is particularly critical in "asymptotic approximation" methods. On the other hand, the over-approximation methods have to be designed based on the characteristics of the specific system under study, and generally provide solutions to the safety verification problem that are too conservative when the system dynamics is complex and the reachable sets have an arbitrary shape. As for the asymptotic approximation methods, they can be applied to general classes of systems and they do not require a specific shape for the reachable sets.

In many control applications, the dynamics of the system under study is subjected to the perturbation of random noises that are either inherent or present in the environment. These systems are naturally described by stochastic models, whose trajectories occur with different probabilities. For this class of systems, one can adopt either a worst-case approach or a probabilistic approach to safety verification. In the worst-case approach to safety verification, one requires all the admissible trajectories of the system to be outside the unsafe set, irrespectively of their probability, thus ignoring the stochastic nature of the system. In [8], for example, the system is stochastic because of some random noise signal affecting the system dynamics. However, the noise process is assumed to be bounded and treated as if it were a deterministic signal taking values in a known compact set for the purpose of reachability computations. In the probabilistic approach to safety verification, one allows some trajectories of the system to enter the unsafe set if this event has low probability, thus avoiding the conservativeness of the worst-case approach. A probabilistic approach to safety verification can be useful within a structured alerting system where alarms of different severity are issued depending on the level of criticality of the situation. For systems operating in a highly dynamic uncertain environment, safety has to be repeatedly verified on-line based on the updated information on the system behavior. In these applications it is then very important to have some measure of criticality for evaluating whether the selected control input is appropriate or a corrective action should be taken to timely steer the system out of the unsafe set. A natural choice for the measure of criticality is the probability of intrusion into the unsafe set within a finite/infinite time horizon: the higher the probability of intrusion, the more critical the situation.

1.2 Application of probabilistic reachability analysis to air traffic management

In this work we study the problem of conflict prediction in Air Traffic Management (ATM) as a probabilistic safety verification problem.

Our objective is to evaluate if the flight plan assigned to an aircraft is "safe" in the sense that by following it the aircraft will not get into any conflict situation. This is done by estimating the probability that a conflict will occur over some look-ahead time horizon. In practice, once a prescribed threshold value of the probability of conflict is surpassed, an alarm of corresponding severity should be issued to the air traffic controllers/pilots to warn them on the level of criticality of the situation [9].

As pointed out in Deliverable 1.1 of the HYBRIDGE project ([10]), there are several operational situations in ATM in which the issue of conflict detection for an aircraft with a given flight plan is safety relevant. In the present work, we study the problem of detecting when following some prescribed flight plan will cause the aircraft to get closer than a certain distance to another aircraft or to enter some forbidden region of the airspace. In the sequel, these flight-plan-level conflicts are shortly referred to as "aircraft-to-aircraft conflict" and "aircraft-to-airspace conflict", respectively. In Deliverable D6.1 ([11, Chapter 3]) under workpackage 6 of the HYBRIDGE project an overview of the aircraft-to-aircraft conflict detection problem in ATM is given. However, no connection is established in D6.1 between conflict detection and probabilistic safety verification,

which is being done in the current report.

Aircraft-to-aircraft conflict: An aircraft-to-aircraft conflict occurs when two aircraft come closer than a minimum prescribed distance. According to the ATM definition, a two aircraft encounter is conflict-free if the two aircraft are either at a horizontal distance greater than r or at a vertical distance greater than H during the whole duration of the encounter, where r and H are prescribed quantities [12]. Currently, $r = 5$ nautical miles (nmi) for en-route airspace and $r = 3$ nmi inside the Terminal Radar Approach Control (TRACON) area, whereas $H = 1000$ feet (ft). If the two aircraft get closer than r horizontally and H vertically at some time instant during the encounter, then, an aircraft-to-aircraft conflict occurs.

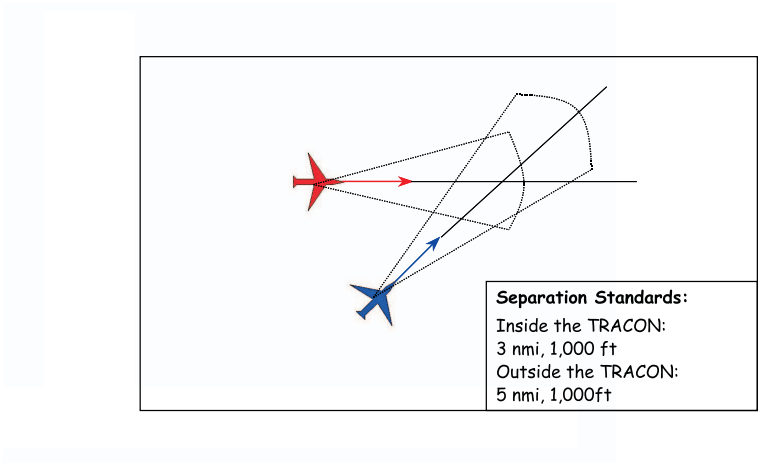

Figure 1: Aircraft-to-aircraft conflict.

Aircraft-to-airspace conflict: An aircraft-to-airspace conflict occurs when an aircraft enters a forbidden area of the airspace. For a variety of reasons, an aircraft trajectory is constrained to limited spaces during a flight. Large sectors of airspace over Europe are "no-go" because of, for example, Special Use Airspace (SUA) areas in the military airspace or separation buffers around strategically important objects. Airspace restrictions can also originate dynamically due to severe weather conditions or high traffic congestion causing some airspace area to exceed its maximal capacity. The management of air traffic as density increases around the restricted areas is then crucial to avoid aircraft-to-airspace conflicts.

We address the problem of conflict probability analysis from the perspective of the current centralized ATM system, where aircraft are prescribed to follow certain flight plans, and Air Traffic Controllers (ATCs) on the ground are responsible of ensuring aircraft safety by issuing trajectory specifications to the pilots.

The procedure used to prevent the occurrence of a conflict in ATM typically consists of two phases, namely, aircraft conflict detection and aircraft conflict resolution. Automated tools are currently being studied to support ATCs in performing these tasks. A comprehensive overview of the methods proposed in the literature for aircraft-to-aircraft conflict detection can be found

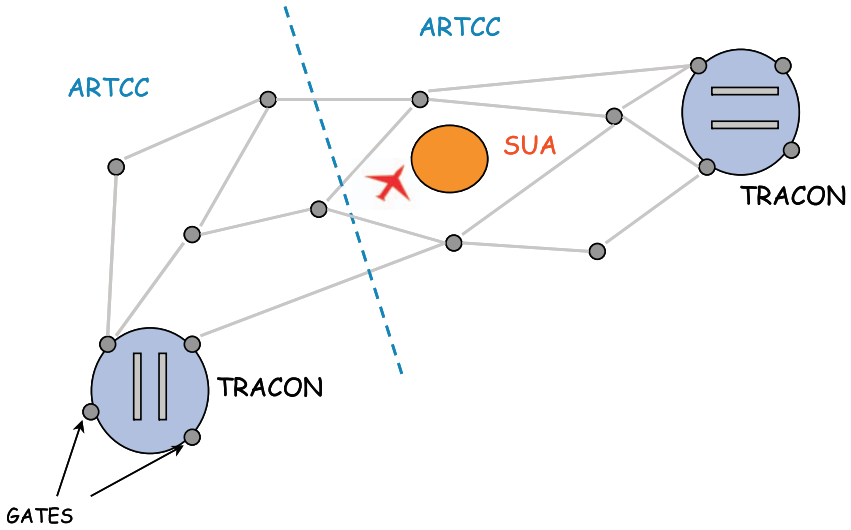

Figure 2: Aircraft-to-airspace conflict: an aircraft is entering a Special Use Area (SUA) while flying in a region of the airspace between two Terminal Radar Approach Control (TRACON) areas, divided into two Air Route Traffic Control Centers (ARTCC).

in [13] .

In automated conflict detection, models for predicting the aircraft future position are introduced and the possibility that a conflict would happen within a certain time horizon is evaluated based on these models ([9]-[16]). If a conflict is predicted, then the aircraft flight plans are modified in the conflict resolution phase so as to avoid the actual occurrence of the predicted conflict. The cost of the resolution action in terms of, for example, delay, fuel consumption, deviation from originally planned itinerary, is usually taken into account when selecting a new flight plan ([17]-[24]).

In this work we focus on the conflict detection issue and address it according to a probabilistic viewpoint. It is important to note that we do not address issues related to a possible discrepancy between the flight plan at the ATC level and that set by the pilot on board of the aircraft. Modeling this aspect would require a more complex stochastic hybrid model than the one introduced here, where the hybrid component of the system is mainly due to changes in the aircraft dynamics at the way-points prescribed by their flight plan. Detecting situation awareness errors in fact requires modeling ATC and pilots by hybrid systems, and building an observer for the overall hybrid system obtained by composing the hybrid models of the agents and the aircraft. This is one of the objectives of workpackage 7 within the HYBRIDGE project.

1.3 Description of the reachability analysis approach to air traffic conflict detection

We consider an aircraft flying in some region of the airspace and suppose that the aircraft is prescribed to follow a certain flight plan. Our objective is evaluating whether the aircraft flight plan is conflict free, or it should be changed to avoid the occurrence of a possible conflict. The

results illustrated here have appeared in [25], [26], and [27].
There are several factors that combined make this conflict analysis problem highly complicated, and as such impossible to solve analytically. Aircraft flight plans can be, in principle, arbitrary motions in the three dimensional airspace, and they are generally more complex than the simple planar linear motions assumed in [15, 28] when determining analytic expressions for the probability of an aircraft-to-aircraft conflict. Also, forbidden airspace areas may have an arbitrary shape, which can also change in time, as, for example, in the case of a storm that covers an area of irregular shape that evolves dynamically. Finally, and probably most importantly, the random perturbation to the aircraft motion is spatially correlated. Wind is the main source of uncertainty on the aircraft position, and if we consider two aircraft, the closer the aircraft, the larger the correlation between the wind perturbations. Although this last factor is known to be critical, it is largely ignored in the current literature on aircraft safety studies, probably because it is difficult to model and analyze. The methods proposed in the literature to compute the probability of conflict are generally based on the description of the aircraft future positions first proposed in [14]. In [14], each aircraft motion is described as a Gaussian random process whose variance grows in time, and the processes modeling the motions of different aircraft are assumed to be uncorrelated. However, this assumption may be unrealistic in practice, and can cause erroneous evaluations of the probability of conflict, since wind is the main source of uncertainty and the correlation between the wind perturbations affecting the aircraft positions is stronger when two aircraft are closer to each other. To our knowledge, the first attempt to model the wind perturbation to the aircraft motion for Air Traffic Management (ATM) applications was done in [29], which inspired this work.

The main contributions reported in this work are:

- the introduction of a class of probabilistic hybrid systems for predicting the aircraft future position along some look-ahead time horizon, and
- the development of an algorithm for reachability computations for the introduced class of systems.

The model for predicting the aircraft future position incorporates the information on the aircraft flight plan, and takes into account the presence of wind as the main source of uncertainty on the aircraft actual motion. More specifically, we assume that each aircraft is trying to follow a flight plan, which typically consists of straight lines between given way points traveled at constant speed. The aircraft actual motion may deviate from the planned motion because of different sources of uncertainty. In particular, we assume that the possible errors in tracking the flight plan are mainly due to the wind influence on the aircraft velocity. We address the general case when the aircraft might change altitude during its flight. Modeling altitude changes is important not only because the aircraft changes altitude when it is inside a TRACON area, but also because altitude changes can be used as resolution maneuvers to avoid, e.g., severe perturbation areas or conflict situations with other aircraft ([12],[30],[21]). Conflicts are typically resolved by resorting to the turn, climb/descend, and accelerate/decelerate actions, which affect the aircraft heading, altitude, and speed, respectively ([21]). It is found that climb/descend is the most efficient action for resolving short-term conflicts. Vertical maneuvers are in fact used to resolve

imminent conflicts in the Traffic Alert and Collision Avoidance System (TCAS [12, 30]).
The proposed class of systems is conceived with the objective of compromising between the two conflicting objectives of being a realistic description of the aircraft motion from the ATM point of view, while maintaining at the same time an appropriate degree of simplicity to allow for theoretical studies. The hybrid nature of the model is due to the change in the dynamics when a way-point is reached. The probabilistic component is due to the wind, which is described by a random field to model the spatial correlation between the wind perturbations to the aircraft motion. To a certain extent, our model can be considered a simplified version of the model in [29], which is in fact interesting but too complicated to conceive a method for computing the probability of conflict based on it.
Based on the aircraft predicted motion, we evaluate if the flight plan assigned to the aircraft is safe by the probability that the prescribed separation requirements from another aircraft or a prohibited airspace area are violated: the lower the probability, the higher the safety level. Analytic, though approximated, expressions for the probability that two aircraft flying at the same altitude get closer than the minimum prescribed distance are given in [15]. These analytic expressions are obtained by reducing the problem to that of estimating the probability that a two-dimensional Brownian motion with constant drift will eventually enter an ellipsoidal region. This requires specific assumptions on the two-aircraft model and the shape of the conflict area, which makes the approach not applicable to the general case addressed here.

The distinguishing feature of the methodology for reachability analysis proposed in this work is that it rests on the approximation of the solution to stochastic differential equations by using Markov chains. The basic idea is to construct a Markov chain whose state space is obtained by discretizing the original space into grids. For properly chosen transition probabilities, the Markov chain converges weakly to the solution to the stochastic differential equation as the discretization step approaches zero. Therefore, an approximation of the probability of interest can be obtained by computing the corresponding quantity for the Markov chain.
From an algorithmic point of view, we propose a backward reachability algorithm which computes for each state an estimate of the probability that the system will enter the unsafe set starting from that state by appropriately propagating the transition probabilities of the Markov chain while it evolves backwards in time starting from the unsafe set during the time horizon of interest.
According to the classification of safety verification approaches mentioned in Section 1.1, our approach can be described as an "asymptotic approximation" probabilistic model checking method based on backward reachability computations.

1.4 Structure of the deliverable

The rest of Deliverable 3.1 is organized as follows. The class of systems modeling the aircraft motion from the ATC point of view is described in Section 2, and the proposed new methodology for reachability analysis of these systems is presented in Section 3. Examples of application of the proposed methodology to safety analysis in aircraft flight are shown in Section 4, whose objective is pointing out the dependence of the probability of the aircraft-to-aircraft conflict on the wind spatial correlation structure. Considerations on computational time, realistic values

for the parameters of the wind statistics, etc., are not included in Section 4. This investigation is part of the work under Deliverable 3.2 on "Probabilistic aircraft conflict detection". Finally, the proposed reachability analysis method is discussed in Section 5, pointing out its limitations, illustrating possible extensions to overcome them, and describing foreseen applications to the design of conflict resolution strategies.

2 Model of the aircraft motion

In this section we introduce a kinematic model of the aircraft motion to predict the aircraft future position during the time interval $T = [0, t_f]$, where 0 is the current time instant, and t_f is a positive real number (possibly infinity) representing the look-ahead time horizon.

The airspace and the aircraft position at time $t \in T$ are $\mathbb{R}^3$ and $X(t) \in \mathbb{R}^3$, respectively. We assume that the flight plan assigned to the aircraft is specified in terms of a velocity profile $u : T \to \mathbb{R}^3$, meaning that at time $t \in T$ the aircraft plans to fly at a velocity $u(t)$. Since, according to the common practice in ATM systems, aircraft are advised to travel at constant speed piecewise linear motions specified by a series of way-points, the velocity profile u is taken to be a piecewise constant function, which causes the resulting model to be hybrid.

We suppose that the main source of uncertainty in the aircraft future position during the time interval T is the wind, which affects the aircraft motion by acting on the aircraft velocity. The wind contribution to the velocity of the aircraft is due to the *wind speed*. Note that here we adopt the ATM terminology and use the word 'speed' for the velocity vector.
The wind speed can be further decomposed into two components: i) a deterministic term representing the nominal wind speed, which may depend on the aircraft location and time t, and is assumed to be known to the ATC through measurements or forecast; and ii) a stochastic term representing the effect of air turbulence and errors in the wind speed measurements and forecast.

As a result of the above discussion, the position X of the aircraft during the time horizon T is governed by the following stochastic differential equation:

$$dX(t) = u(t)dt + f(X,t)dt + \Sigma(X,t)dB(X,t), \tag{1}$$

initialized with the aircraft current position $X(0)$.

We next explain the different terms appearing in equation (1).

First of all, $f : \mathbb{R}^3 \times T \to \mathbb{R}^3$ is a time-varying vector field on $\mathbb{R}^3$: for a fixed $(x,t) \in \mathbb{R}^3 \times T$, $f(x,t)$ represents the nominal wind speed at position x and at time t. We call f the *wind field*.

$B(\cdot,\cdot)$ is a time-varying random field on $\mathbb{R}^3 \times T$ modeling (the integral of) air turbulence perturbations to aircraft velocity as well as wind speed forecast errors. It can be thought of as the time integral of a Gaussian random field correlated in space and uncorrelated in time. Formally, $B(\cdot,\cdot)$ has the following properties:

i) for each fixed $x \in \mathbb{R}^3$, $B(x,\cdot)$ is a standard 3-dimensional Brownian motion. Hence $dB(x,t)/dt$ can be thought of as a 3-dimensional white noise process;

ii) $B(\cdot,\cdot)$ is time increment independent. This implies, in particular, that the collections of random variables $\{B(x,t_2) - B(x,t_1)\}_{x\in\mathbb{R}^3}$ and $\{B(x,t_4) - B(x,t_3)\}_{x\in\mathbb{R}^3}$ are independent for any $t_1, t_2, t_3, t_4 \in T$, with $t_1 \le t_2 \le t_3 \le t_4$;

iii) for any $t_1, t_2 \in T$ with $t_1 \le t_2$, $\{B(x,t_2) - B(x,t_1)\}_{x\in\mathbb{R}^3}$ is an (uncountable) collection of Gaussian random variables with zero mean and covariance

$$E\big\{[B(x,t_2) - B(x,t_1)][B(y,t_2) - B(y,t_1)]^T\big\} = \rho(x-y)(t_2-t_1)I_3,\ \forall x, y \in \mathbb{R}^3,$$

where I_3 is the 3-by-3 identity matrix, and $\rho : \mathbb{R}^3 \to \mathbb{R}$ is a continuous function with $\rho(0) = 1$ and $\rho(x)$ decreases to zero as $x \to \infty$. In addition, ρ has to be non-negative definite in the sense that the k-by-k matrix $[\rho(x_i - x_j)]_{i,j=1}^k$ is non-negative definite for arbitrary $x_1, \ldots, x_k \in \mathbb{R}^3$ and positive integer k. See [31] for other equivalent conditions of this non-negative definite requirement.

Remark 1 *Typically the wind field f is supposed to satisfy some continuity property. This condition, together with the monotonicity assumption on the spatial correlation function ρ, is introduced to model the fact that the closer two points in space, the more similar the wind speeds at those points, and, as the two points move farther away from each other, their wind speeds become more and more independent.*

The spatial correlation function $\rho : \mathbb{R}^3 \to \mathbb{R}$ can be taken to be $\rho(x) = \exp(-c_h \|x\|_h - c_v \|x\|_v)$ for some $c_v \geq c_h > 0$, where the subscripts h and v stand for "horizontal" and "vertical", and $\|(x_1, x_2, x_3)\|_h \triangleq \sqrt{x_1^2 + x_2^2}$ and $\|(x_1, x_2, x_3)\|_v \triangleq |x_3|$ for any $(x_1, x_2, x_3) \in \mathbb{R}^3$. This is to model the fact that the wind correlation in space is weaker in the vertical direction.

Exponentially decaying spatial correlation functions are a popular choice for random field models in geostatistics [32]. This choice is actually suitable for ATM applications. In [33], the wind field prediction made by the Rapid Update Cycle (RUC [34]) developed at the National Oceanic and Atmospheric Administration (NOAA) Forecast System Laboratory (FOL) is compared with the empirical data collected by the Meteorological Data Collection Reporting System (MDCRS) near Denver International Airport. The result of this comparison is that the spatial correlation statistics of the wind field prediction errors is adequately described by an exponentially decaying function of the horizontal separation.

As a random field, $B(\cdot, \cdot)$ is Gaussian, stationary in space (its finite dimensional distributions remain unchanged when the origin of $\mathbb{R}^3$ is shifted), and isotropic in the horizontal directions (its finite dimensional distributions are invariant with respect to changes of orthonormal coordinates in the horizontal directions).

Finally, $\Sigma : \mathbb{R}^3 \times T \to \mathbb{R}^{3\times 3}$ modulates the variance of the random perturbation to the aircraft velocity. We assume that $\Sigma(\cdot, \cdot)$ is a constant diagonal matrix Σ given by $\Sigma \triangleq \mathrm{diag}(\sigma_h, \sigma_h, \sigma_v)$, for some constant $\sigma_h, \sigma_v > 0$. Note that after the modulation of Σ the random contribution of the wind to the aircraft velocity remains isotropic horizontally. However, its variance in the vertical direction can be different from that in the horizontal ones.
Equation (1) can then be rewritten as

$$dX(t) = u(t)dt + f(X, t)dt + \Sigma\, dB(X, t) \tag{2}$$

with initial condition $X(0)$.

Based on model (2) of the aircraft motion, we shall derive the equations to study the aircraft-to-aircraft and aircraft-to-airspace problems.

Note that this simplified model of the aircraft motion does not take into account the feedback control action of the flight management system (FMS), which tries to reduce the tracking error with respect to the planned trajectory. However, the methodology for reachability computations

described based on this model can be extended to address also the case when a model of the FMS is included. A discussion on this is postponed to Section 5.

2.1 Aircraft-to-aircraft conflict problem

Consider two aircraft, say "aircraft 1" and "aircraft 2", flying in the same region of the airspace during the time interval $T = [0, t_f]$. If the two aircraft get closer than r horizontally and H vertically at some $t \in T$, then, an aircraft-to-aircraft conflict occurs.

Denote the position of aircraft 1 and aircraft 2 by X_1 and X_2, respectively. Based on (2), the evolutions of $X_1(\cdot)$ and $X_2(\cdot)$ over the time interval T are governed by

$$dX_1(t) = u_1(t)dt + f(X_1, t)dt + \Sigma\, dB(X_1, t), \tag{3}$$

$$dX_2(t) = u_2(t)dt + f(X_2, t)dt + \Sigma\, dB(X_2, t), \tag{4}$$

starting from the initial positions $X_1(0)$ and $X_2(0)$.

The probability of conflict can be expressed in terms of the relative position $Y \triangleq X_2 - X_1$ of the two aircraft as

$$P\{Y(t) \in \mathcal{D} \text{ for some } t \in T\}, \tag{5}$$

where $\mathcal{D} \in \mathbb{R}^3$ is the closed cylinder of radius r and height $2H$ centered at the origin.

2.1.1 Affine case

In this section we consider the case when the wind field $f(x, t)$ is affine in x, i.e.,

$$f(x, t) = R(t)x + d(t), \quad \forall x \in \mathbb{R}^3,\, t \in T,$$

where $R : T \to \mathbb{R}^{3\times 3}$ and $d : T \to \mathbb{R}^3$ are continuous functions. We shall show that in this case we can refer to a simplified model for the two aircraft system to compute the probability of conflict.

The relative position Y and the nominal relative velocity v of aircraft 1 and aircraft 2 are respectively given by

$$Y \triangleq X_2 - X_1, \quad v \triangleq u_2 - u_1.$$

Since the positions of the two aircraft, X_1 and X_2, are governed by equations (3) and (4), by subtracting (3) from (4), we have

$$dY(t) = v(t)dt + R(t)Y(t)dt + \Sigma d[B(X_2, t) - B(X_1, t)]. \tag{6}$$

$B(\cdot, \cdot)$ can be rewritten in the Karthunen-Loeve expansion as

$$B(x, t) = \sum_{n=0}^{\infty} \sqrt{\lambda_n}\phi_n(x)B_n(t),$$

where $\{B_n(t)\}_{n\geq 0}$ is a series of independent three-dimensional standard Brownian motions, and $\{(\lambda_n, \phi_n(x))\}_{n\geq 0}$ is a complete set of eigenvalue and eigenfunction pairs for the integral operator $\phi(x) \mapsto \int_{\mathbb{R}^3} \rho(s-x)\phi(s)\,ds$, i.e.,

$$\begin{cases} \lambda_n \phi_n(x) = \int_{\mathbb{R}^3} \rho(s-x)\phi_n(s)\,ds, \\ \rho(x-y) = \sum_{n=0}^{\infty} \lambda_n \phi_n(x)\phi_n(y), \end{cases} \quad \forall x, y \in \mathbb{R}^3. \tag{7}$$

Fix $x_1, x_2 \in \mathbb{R}^3$ and let $y = x_2 - x_1$. Define

$$Z(t) \triangleq [B(x_2,t) - B(x_1,t)] = \sum_{n=0}^{\infty} \sqrt{\lambda_n}[\phi_n(x_2) - \phi_n(x_1)]B_n(t). \tag{8}$$

$Z(t)$ is a Gaussian process with zero mean and covariance

$$E\{[Z(t_2) - Z(t_1)][Z(t_2) - Z(t_1)]^T\} = 2[1-\rho(y)](t_2 - t_1)I_3, \quad \forall t_1 \leq t_2,$$

where the last equation follows from (7) and the fact that $\rho(0) = 1$. Note also that $Z(0) = 0$. Therefore, in terms of distribution we have

$$Z(t) \stackrel{d}{=} \sqrt{2[1-\rho(y)]}\, W(t), \tag{9}$$

where $W(t)$ is a standard 3-dimensional Brownian motion.

As a result, (6) can then be approximated weakly by

$$dY(t) = v(t)dt + R(t)Y(t)dt + \sqrt{2[1-\rho(Y)]}\Sigma\, dW(t). \tag{10}$$

By this we mean that the stochastic process $Y(t) = X_2(t) - X_1(t)$ obtained by subtracting the solution to (3) from the solution to (4) initialized respectively with $X_1(0)$ and $X_2(0)$ has the same distribution as the solution to (10) initialized with $Y(0) = X_2(0) - X_1(0)$.

2.1.2 General case

If no assumption is made on the wind field $f(x,t)$, to compute the probability of conflict (5), it no longer suffices to consider only the relative position of the two aircraft as in the previous section. Instead, we have to keep track of the two aircraft positions.

Define

$$\hat{X} = \begin{bmatrix} X_1 \\ X_2 \end{bmatrix} \in \mathbb{R}^6.$$

Then equations (3) and (4) can be written in terms of $\hat{X}$ as a single equation:

$$d\hat{X}(t) = \hat{u}(t)dt + \hat{f}(\hat{X},t)dt + \hat{\Sigma}d\hat{B}(\hat{X},t), \tag{11}$$

where we set

$$\hat{\Sigma} \triangleq \begin{bmatrix} \Sigma & 0 \\ 0 & \Sigma \end{bmatrix}, \quad \hat{u}(t) = \begin{bmatrix} u_1(t) \\ u_2(t) \end{bmatrix}, \quad \hat{f}(\hat{X},t) = \begin{bmatrix} f(X_1,t) \\ f(X_2,t) \end{bmatrix}, \quad \hat{B}(\hat{X},t) = \begin{bmatrix} B(X_1,t) \\ B(X_2,t) \end{bmatrix}, \quad t \in T.$$

Fix $\hat{x} \in \mathbb{R}^6$. Let $\hat{Z}(t) \triangleq \hat{\Sigma}\,\hat{B}(\hat{x}, t)$. $\{\hat{Z}(t), t \geq 0\}$ is a Gaussian process with zero mean and covariance

$$E[\hat{Z}(t)\hat{Z}(t)^T] = \begin{bmatrix} t\,I_3 & \hat{\rho}(\hat{x})\,t\,I_3 \\ \hat{\rho}(\hat{x})\,t\,I_3 & t\,I_3 \end{bmatrix} \hat{\Sigma}^2,$$

with $\hat{\rho}(\hat{x}) \triangleq \rho(x_1 - x_2)$, with $\hat{x} = (x_1, x_2)$. Analogously to the analysis in the previous section, we can show that, in terms of distribution,

$$\hat{Z}(t) \stackrel{d}{\simeq} \sigma(\hat{x})\hat{\Sigma}\,\hat{W}(t),$$

where $\hat{W}(t)$ is a standard Brownian motion in $\mathbb{R}^6$, and

$$\sigma(\hat{x}) \triangleq \begin{bmatrix} I_3 & \hat{\rho}(\hat{x})\,I_3 \\ \hat{\rho}(\hat{x})\,I_3 & I_3 \end{bmatrix}^{1/2} \in \mathbb{R}^{6\times 6}.$$

As a result, (11) becomes

$$d\hat{X}(t) = \hat{u}(t)dt + \hat{f}(\hat{X}, t)dt + \sigma(\hat{X})\hat{\Sigma}\,d\hat{W}(t). \tag{12}$$

2.2 Aircraft-to-airspace conflict problem

Consider an aircraft flying in some region of the airspace, close to a certain prohibited area such as, e.g., a special usage area or a severe weather zone. An aircraft-to-airspace conflict occurs if the aircraft enters the prohibited area within the look-ahead time horizon T. If this area can be described by a set $\mathcal{D} \subset \mathbb{R}^3$, then this problem can be formulated as the estimation of the probability

$$P\{X(t) \in \mathcal{D} \text{ for some } t \in T\} \tag{13}$$

where $X(t)$ is the aircraft position at time $t \in T$ and is obtained by (2) initialized with $X(0)$.

Note that we are considering a single aircraft, and, for each fixed $x \in \mathbb{R}^n$, $B(x, \cdot)$ is a standard 3-dimensional Brownian motion, and $B(\cdot, \cdot)$ is time increment independent and stationary. We can then replace $B(\cdot, \cdot)$ with a standard Brownian motion $W(\cdot)$, and refer to

$$dX(t) = u(t)dt + f(X, t)dt + \Sigma\,dW(t), \tag{14}$$

initialized with $X(0)$, for the purpose of computing the probability in (13).

3 The proposed method for probabilistic safety verification

In this section we describe a method for estimating the probability that the solution over the time interval $T = [0, t_f]$ to the stochastic differential equation

$$dS(t) = a(S,t)dt + b(S)\Gamma\, dW(t) \tag{15}$$

with initial condition $S(0)$ enters a certain compact set $\mathcal{D}$:

$$P\{S(t) \in \mathcal{D} \text{ for some } t \in T\}. \tag{16}$$

Function $a : \mathbb{R}^n \times T \to \mathbb{R}^n$ is the drift term, function $b : \mathbb{R}^n \to \mathbb{R}^{n\times n}$ is the diffusion term, and Γ is a diagonal matrix with positive entries, which modulates the variance of the standard n-dimensional Brownian motion $W(\cdot)$. With reference to the models introduced in Section 2, when studying the criticality of a two aircraft encounter, S represents either the aircraft relative position (Section 2.1.1) or the two aircraft positions (Section 2.1.2), depending on the wind field structure, whereas, when evaluating the possible occurrence of an aircraft-to-airspace conflict, S represents the aircraft position (Section 2.2).
In the analysis to follow, we assume that $b : \mathbb{R}^n \to \mathbb{R}^{n\times n}$ is a continuous function, whereas $a : \mathbb{R}^n \times T \to \mathbb{R}^n$ is continuous in its first argument and only piecewise continuous in its second argument. Note that, under these assumptions, the aircraft-to-aircraft and aircraft-to-airspace safety analysis problems can be seen as particular cases of the problem addressed in this section. Indeed, (10), (12), and (14) reduce to (15) for appropriately chosen a and b functions, with the discontinuity in a caused by the discontinuity in the aircraft flight plan at the prescribed timed way-points. Since in the ATM application of interest, $\mathcal{D}$ represents an unsafe region where a conflict takes place, in the sequel we shall refer to the quantity in (16) as the *probability of conflict*.

To evaluate the probability of conflict (16) numerically, we consider an open domain $\mathcal{U} \subset \mathbb{R}^n$ that contains $\mathcal{D}$ and has compact support. $\mathcal{U}$ should be large enough so that the situation can be declared safe once S ends up outside $\mathcal{U}$. With reference to the domain $\mathcal{U}$, the probability of entering the unsafe set $\mathcal{D}$ can be expressed as

$$P_c \triangleq P\{S \text{ hits } \mathcal{D} \text{ before hitting } \mathcal{U}^c \text{ within the time interval } T\}, \tag{17}$$

where $\mathcal{U}^c$ denotes the complement of $\mathcal{U}$ in $\mathbb{R}^n$. Implicit in the above definition is that if S hits neither $\mathcal{D}$ nor $\mathcal{U}^c$ during T, no conflict occurs.
For the purpose of computing (17), we can assume that in equation (15), S is defined on the open domain $\mathcal{U} \setminus \mathcal{D}$ with initial condition $S(0)$, and that it is stopped as soon as it hits the boundary $\partial\mathcal{U} \cup \partial\mathcal{D}$.

3.1 Markov chain approximation: weak convergence result

We now describe an approach to approximate the solution $S(\cdot)$ to equation (15) defined on $\mathcal{U} \setminus \mathcal{D}$ with absorption on the boundary $\partial\mathcal{U} \cup \partial\mathcal{D}$. The idea is to discretize $\mathcal{U} \setminus \mathcal{D}$ into grid points that constitute the state space of a Markov chain. By carefully choosing the transition

probabilities, the solution to the Markov chain will converge weakly to that of the stochastic differential equation (15) as the grid size approaches zero. Therefore, at a small grid size, a good estimate of the probability P_c in (17) is provided by the corresponding quantity associated with the Markov chain, which is much easier to compute.

To define the Markov chain, we first need to introduce some notations.
Let

$$\Gamma = \mathrm{diag}(\sigma_1, \sigma_2, \ldots, \sigma_n),$$

with $\sigma_1, \sigma_2, \ldots, \sigma_n > 0$.

Fix a grid size $\delta > 0$. Denote by $\delta\mathbb{Z}^n$ the integer grids of $\mathbb{R}^n$ scaled properly, more precisely,

$$\delta\mathbb{Z}^n = \{(m_1\eta_1\delta, m_2\eta_2\delta, \ldots, m_n\eta_n\delta) |\ (m_1, m_2, \ldots, m_n) \in \mathbb{Z}^n\},$$

where η_i, $i = 1, \ldots, n$, are defined as

$$\eta_i \triangleq \frac{\sigma_i}{\bar{\sigma}},\ i = 1, \ldots, n,$$

with $\bar{\sigma} = \max_i \sigma_i$. For each grid point $q \in \delta\mathbb{Z}^n$, define the immediate neighbors set

$$\mathcal{N}_q = \{q + (i_1\eta_1\delta, i_2\eta_2\delta, \ldots, i_n\eta_n\delta) |\ (i_1, i_2, \ldots, i_n) \in \mathcal{I}\}, \tag{18}$$

where $\mathcal{I} \subseteq \{0, 1, -1\}^n \setminus \{(0, 0, \ldots, 0)\}$. The immediate neighbors set $\mathcal{N}_q$ is a subset of all the points in $\delta\mathbb{Z}^n$ whose distance from q along the coordinate axis x_i is at most $\eta_i\delta$, $i = 1, \ldots, n$. The larger the cardinality of $\mathcal{N}_q$, the more intensive the computations. For the convergence result to hold, different choices for $\mathcal{N}_q$ are possible, which depend, in particular, on the diffusion term b in (15). For the time being, consider the immediate neighbors set as given. We shall then see possible choices for it in the cases of interest in aircraft flight safety analysis.

Define $\mathcal{Q} = (\mathcal{U} \setminus \mathcal{D}) \cap \delta\mathbb{Z}^n$, which consists of all those grid points in $\delta\mathbb{Z}^n$ that lie inside $\mathcal{U}$ but outside $\mathcal{D}$. The interior of $\mathcal{Q}$, denoted by $\mathcal{Q}^0$, consists of all those points in $\mathcal{Q}$ which have all their neighbors in $\mathcal{Q}$. The boundary of $\mathcal{Q}$ is defined to be $\partial\mathcal{Q} = \mathcal{Q} \setminus \mathcal{Q}^0$, and is the union of two disjoint sets: $\partial\mathcal{Q} = \partial\mathcal{Q}_\mathcal{U} \cup \partial\mathcal{Q}_\mathcal{D}$, where points in $\partial\mathcal{Q}_\mathcal{U}$ have at least one neighbor outside $\mathcal{U}$, and points in $\partial\mathcal{Q}_\mathcal{D}$ have at least one neighbor inside $\mathcal{D}$. If a point satisfies both the conditions, then we assign it only to $\partial\mathcal{Q}_\mathcal{D}$. This will eventually lead to an overestimation of the probability of conflict. However, if $\mathcal{U}$ is chosen to be large enough, the overestimation error is negligible.

We now define a Markov chain $\{Q_k,\ k \geq 0\}$ on the state space $\mathcal{Q}$. Denote by $\Delta t > 0$ the amount of time elapsing between any two successive discrete time steps k and $k+1$, $k \geq 0$. $\{Q_k,\ k \geq 0\}$ is a time-inhomogeneous Markov chain such that:

1. each state in $\partial\mathcal{Q}$ is an absorbing state, i.e., the state of the chain remains unchanged after it hits any of the states $q \in \partial\mathcal{Q}$:

$$P\{Q_{k+1} = q' |\ Q_k = q\} = \begin{cases} 1, & q' = q \\ 0, & \text{otherwise} \end{cases}$$

2. starting from a state q in $\mathcal{Q}^0$, the chain jumps to one of its neighbors $\mathcal{N}_q$ or stays at the same state according to transition probabilities determined by its current location q and the current time step k:

$$P\{Q_{k+1} = q' \,|\, Q_k = q\} = \begin{cases} p^k_{q'}(q), & q' \in \mathcal{N}_q \cup \{q\} \\ 0, & \text{otherwise,} \end{cases} \tag{19}$$

where $p^k_{q'}(q)$ are functions of the drift and diffusion terms evaluated at q and time $k\Delta t$.

Set $\Delta t = \lambda\delta^2$, where λ is some positive constant.

Let the Markov chain be at state $q \in \mathcal{Q}^0$ at some time step k. Define

$$m^k_q = \frac{1}{\Delta t} E\{Q_{k+1} - Q_k \,|\, Q_k = q\},$$

$$V^k_q = \frac{1}{\Delta t} E\{(Q_{k+1} - Q_k)(Q_{k+1} - Q_k)^T \,|\, Q_k = q\}.$$

Suppose that as $\delta \to 0$,

$$\begin{aligned} m^k_q &\to a(s, k\Delta t) \\ V^k_q &\to b(s)\Gamma^2 b(s)^T \end{aligned} \tag{20}$$

$\forall s \in \mathcal{U} \setminus \mathcal{D}$, where for each $\delta > 0$ q is a point in $\mathcal{Q}^0$ closest to s.

If the chain $\{Q_k, k \geq 0\}$ starts from a point $\bar{q} \in \mathcal{Q}^0$ closest to $S(0)$, then by Theorem 8.7.1 in [35] (see also [36]), we conclude that

Proposition 1 *Fix $\delta > 0$ and consider the corresponding Markov chain $\{Q_k, k \geq 0\}$. Denote by $\{Q(t), t \geq 0\}$ the stochastic process that is equal to Q_k on the time interval $[k\Delta t, (k+1)\Delta t)$ for all k, where $\Delta t = \lambda\delta^2$. Suppose that as $\delta \to 0$, the equations (20) are satisfied. Then as $\delta \to 0$, $\{Q(t), t \geq 0\}$ converges weakly to the solution $\{S(t), t \geq 0\}$ to equation (15) defined on $\mathcal{U} \setminus \mathcal{D}$ with absorption on the boundary $\partial\mathcal{U} \cup \partial\mathcal{D}$.*

Remark 2 *As the grid size δ decreases, the time interval between consecutive discrete time steps has to decrease for the stochastic process $S(\cdot)$ to be approximated by a Markov chain with one-step successors limited to the immediate neighbors set. It is then not surprising that the time interval Δt is a decreasing function of the grid size δ for the convergence result to hold.*

Let $k_f \triangleq \lfloor \frac{t_f}{\Delta t} \rfloor$ be the largest integer not exceeding $t_f/\Delta t$ ($k_f = \infty$ if $t_f = \infty$). As a result of Proposition 1, a good approximation to the probability of conflict P_c in (17) is given by

$$P_{c,\delta} \triangleq P\{Q_{k_f} \in \partial\mathcal{Q}_{\mathcal{D}}\} = P\{Q_k \text{ hits } \partial\mathcal{Q}_{\mathcal{D}} \text{ before hitting } \partial\mathcal{Q}_{\mathcal{U}} \text{ within } 0 \leq k \leq k_f\}, \tag{21}$$

with the chain $\{Q_k, k \geq 0\}$ starting from a point $\bar{q} \in \mathcal{Q}$ closest to $S(0)$, for a small δ.

A schematic view of the algorithm is represented in Figure 3 for the case $n = 3$. In this figure, the symbol $\xrightarrow{d}$ is used for "convergence in distribution".

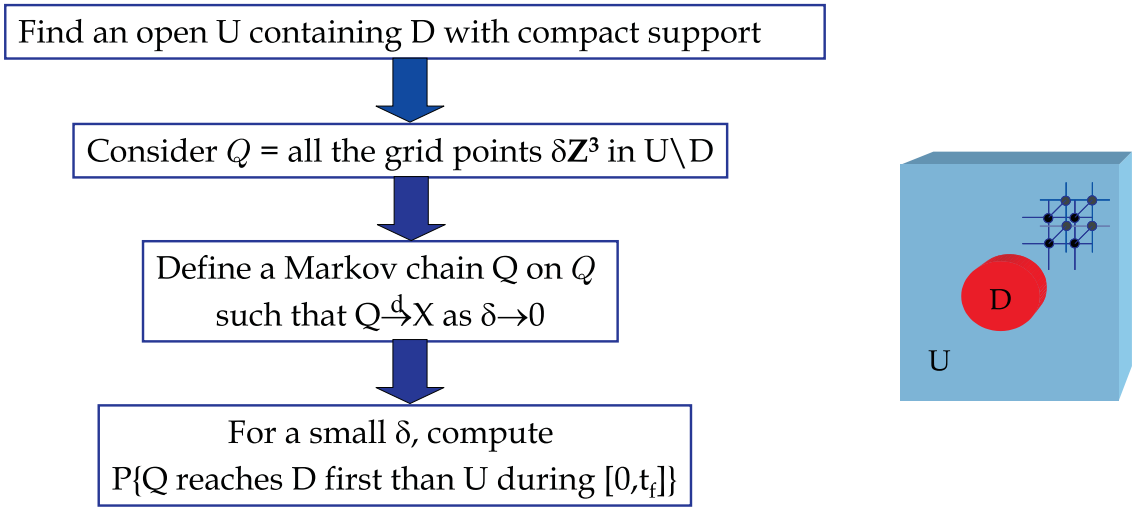

Figure 3: Stochastic approximation algorithm for computing the probability of conflict in the three dimensional case.

3.2 Application to conflict detection in air traffic management

In this section, we describe a possible choice for the immediate neighbors set and the transition probabilities that is effective in guaranteeing that equations (20) (and, hence, the converge result) hold. We distinguish between two different structures of the diffusion term b, the first one suitable for the analysis of aircraft-to-aircraft conflict in the affine case and aircraft-to-airspace conflict, and the second one for the analysis of aircraft-to-aircraft conflict in the general case.

3.2.1 Aircraft-to-aircraft conflict (affine case) and aircraft-to airspace conflict

Suppose that the matrix b in equation (15) has the following form: $b(s) = \beta(s)I$, where $\beta : \mathbb{R}^n \to \mathbb{R}$, which is the case of interest when evaluating the possibility of occurrence of either an aircraft-to-airspace conflict ($\beta(s) = 1$, $\forall s$) or an aircraft-to-aircraft conflict in the affine case ($\beta(s) = \sqrt{2(1-\rho(s)}$, $\forall s$).

Equation (15) then takes the form:

$$dS(t) = a(S,t)dt + \beta(S)\Gamma dW(t).$$

Since each component of the n-dimensional Brownian motion $W(\cdot)$ directly affects a single component of $S(\cdot)$, the immediate neighbors set $\mathcal{N}_q$, $q \in \delta\mathbb{Z}^n$, can be taken as the set of points along the x_i, $i = 1,\dots,n$, directions whose distance from q is $\eta_i\delta$, $i = 1,\dots,n$, respectively. For each $q \in \delta\mathbb{Z}^n$, $\mathcal{N}_q$ is then composed of the following $2n$ elements:

$$\begin{aligned} q_{1_+} &= q + (+\eta_1\delta, 0, \dots, 0), & q_{1_-} &= q + (-\eta_1\delta, 0, \dots, 0), \\ q_{2_+} &= q + (0, +\eta_2\delta, \dots, 0), & q_{2_-} &= q + (0, -\eta_2\delta, \dots, 0), \\ &\vdots & &\vdots \end{aligned}$$

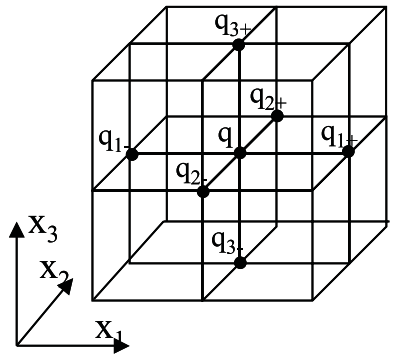

Figure 4: Neighboring grid points in the three dimensional case.

$$q_{n_+} = q + (0, 0, \ldots, +\eta_n \delta), \qquad\qquad q_{n_-} = q + (0, 0, \ldots, -\eta_n \delta),$$

Figure 4 plots the case when $n = 3$. Each grid point has six immediate neighbors (q_{1_-}, q_{1_+}, q_{2_-}, q_{2_+}, q_{3_-}, and q_{3_+}): two (q_{1_-} and q_{1_+}) at a distance $\eta_1\delta$ along direction x_1, two (q_{2_-} and q_{2_+}) at a distance $\eta_2\delta$ along direction x_2, and two (q_{3_-} and q_{3_+}) at a distance $\eta_3\delta$ along direction x_3.

We now define the transition probabilities in (19):

If $q \in \mathcal{Q}^0$, then

$$P\{Q_{k+1} = q' | \, Q_k = q\} = \begin{cases} p_0^k(q) = \dfrac{\xi_0^k(q)}{C_q^k}, & q' = q \\ p_{1_+}^k(q) = \dfrac{\exp(\delta \xi_1^k(q))}{C_q^k}, & q' = q_{1_+} \\ p_{1_-}^k(q) = \dfrac{\exp(-\delta \xi_1^k(q))}{C_q^k}, & q' = q_{1_-} \\ p_{2_+}^k(q) = \dfrac{\exp(\delta \xi_2^k(q))}{C_q^k}, & q' = q_{2_+} \\ p_{2_-}^k(q) = \dfrac{\exp(-\delta \xi_2^k(q))}{C_q^k}, & q' = q_{2_-} \\ \vdots & \\ p_{n_-}^k(q) = \dfrac{\exp(\delta \xi_n^k(q))}{C_q^k}, & q' = q_{n_+} \\ p_{n_-}^k(q) = \dfrac{\exp(-\delta \xi_n^k(q))}{C_q^k}, & q' = q_{n_-} \\ 0, & \text{otherwise,} \end{cases} \tag{22}$$

where

$$\xi_0^k(q) = \frac{2}{\lambda \bar{\sigma}^2 \beta(q)^2} - 2n$$

$$\xi_i^k(q) = \frac{[a(q, k\Delta t)]_i}{\eta_i \bar{\sigma}^2 \beta(q)^2}, \quad i = 1, \ldots, n$$

$$C_q^k = 2\sum_{i=1}^{n} \mathrm{csh}(\delta\xi_i^k(q)) + \xi_0^k(q).$$

λ is a positive constant that has to be chosen small enough such that $\xi_0^k(q)$ defined above is positive for all $q \in \mathcal{Q}$ and all $k \geq 0$. In particular, this is guaranteed if

$$0 < \lambda \leq (n\sigma_1^2 \max_{s \in \mathcal{U}\setminus\mathcal{D}} \beta(s)^2)^{-1}. \tag{23}$$

As for Δt, we set

$$\Delta t = \lambda\delta^2.$$

A direct computation shows that, with this choice for the neighboring set, the transition probabilities, and Δt, for each $q \in \mathcal{Q}^0$ and $k \geq 0$

$$m_q^k = \frac{2}{\lambda\delta C_q^k}\begin{bmatrix} \eta_1 \,\mathrm{sh}(\delta\xi_1^k(q)) \\ \eta_2 \,\mathrm{sh}(\delta\xi_2^k(q)) \\ \vdots \\ \eta_n \,\mathrm{sh}(\delta\xi_n^k(q)) \end{bmatrix}$$

$$V_q^k = \frac{2}{\lambda C_q^k}\,\mathrm{diag}(\eta_1^2\,\mathrm{csh}\left(\delta\xi_1^k(q)\right), \eta_2^2\,\mathrm{csh}(\delta\xi_2^k(q)), \ldots, \eta_n^2\,\mathrm{csh}(\delta\xi_n^k(q))\Big).$$

It is then easily verified that the equations in (20) are satisfied, which in turn leads to the weak convergence result in Proposition 1.

3.2.2 Aircraft-to-aircraft conflict (general case)

When evaluating the criticality of a two-aircraft encounter in the general case, S represents the two aircraft positions, hence the dimension of S is even. Also matrix $\Gamma = \mathrm{diag}(\sigma_1, \sigma_2, \ldots, \sigma_n)$ satisfies $\sigma_h = \sigma_{h+n/2} > 0$, $h = 1, \ldots, n/2$. Moreover, the diffusion term b in equation (15) takes the following form

$$b(s) = \begin{bmatrix} I & \alpha(s)\, I \\ \alpha(s)\, I & I \end{bmatrix}^{1/2}$$

with $\alpha : \mathbb{R}^n \to [0, 1]$. The components h and $h + n/2$ of $S(\cdot)$ are then both directly affected only by the components h and $h+n/2$ of $W(\cdot)$, for every $h = 1, 2, \ldots, n/2$. Based on this observation, the immediate neighbors set $\mathcal{N}_q$, $q \in \delta\mathbb{Z}^n$, can be chosen as follows:

$$\mathcal{N}_q = \{q + (i_1\eta_1\delta, i_2\eta_2\delta, \ldots, i_n\eta_n\delta) |\ (i_1, i_2, \ldots, i_n) \in \mathcal{I}\},$$

where $\mathcal{I} = \{(i_1, i_2, \ldots, i_n) |\ \exists h$ such that $i_h = \pm 1, i_{h+n/2} = \pm 1, i_j = 0, \forall j \neq h, h + n/2\}$. The $2n$ elements of $\mathcal{N}_q$ have the following expression

$$\begin{aligned} q_{1_{++}} &= q + (+\eta_1\delta, 0, \ldots, 0, +\eta_1\delta, 0, \ldots, 0) \\ q_{1_{--}} &= q + (-\eta_1\delta, 0, \ldots, 0, -\eta_1\delta, 0, \ldots, 0) \\ q_{1_{+-}} &= q + (+\eta_1\delta, 0, \ldots, 0, -\eta_1\delta, 0, \ldots, 0) \end{aligned}$$

$$
\begin{aligned}
q_{1_{-+}} &= q + (-\eta_1\delta, 0, \ldots, 0, +\eta_1\delta, 0, \ldots, 0)\\
q_{2_{++}} &= q + (0, +\eta_2\delta, \ldots, 0, 0, +\eta_2\delta, \ldots, 0)\\
q_{2_{--}} &= q + (0, -\eta_2\delta, \ldots, 0, 0, -\eta_2\delta, \ldots, 0)\\
q_{2_{+-}} &= q + (0, +\eta_2\delta, \ldots, 0, 0, -\eta_2\delta, \ldots, 0)\\
q_{2_{-+}} &= q + (0, -\eta_2\delta, \ldots, 0, 0, +\eta_2\delta, \ldots, 0)\\
&\vdots\\
q_{(n/2)_{++}} &= q + (0, 0, \ldots, 0, +\eta_{n/2}\delta, \ldots, 0, 0, \ldots, 0, +\eta_{n/2}\delta)\\
q_{(n/2)_{--}} &= q + (0, 0, \ldots, 0, -\eta_{n/2}\delta, \ldots, 0, 0, \ldots, 0, -\eta_{n/2}\delta)\\
q_{(n/2)_{+-}} &= q + (0, 0, \ldots, 0, +\eta_{n/2}\delta, \ldots, 0, 0, \ldots, 0, -\eta_{n/2}\delta)\\
q_{(n/2)_{-+}} &= q + (0, 0, \ldots, 0, -\eta_{n/2}\delta, \ldots, 0, 0, \ldots, 0, +\eta_{n/2}\delta),
\end{aligned}
$$

where we used the fact that

$$
\eta_i = \frac{\sigma_i}{\bar{\sigma}} = \frac{\sigma_{i+n/2}}{\bar{\sigma}} = \eta_{i+n/2},\ i = 1, \ldots, n/2.
$$

We now define the transition probabilities in (19):

If $q \in \mathcal{Q}^0$, then

$$
P\{Q_{k+1} = q' \,|\, Q_k = q\} = \begin{cases}
p_0^k(q) = \dfrac{\xi_0^k(q)}{C}, & q' = q\\
p_{1_{++}}^k(q) = \dfrac{(1+\alpha(q))\exp(\delta\xi_{1_{++}}^k(q))}{C\,\mathrm{csh}(\delta\xi_{1_{++}}^k(q))}, & q' = q_{1_{++}}\\
p_{1_{--}}^k(q) = \dfrac{(1+\alpha(q))\exp(-\delta\xi_{1_{++}}^k(q))}{C\,\mathrm{csh}(\delta\xi_{1_{++}}^k(q))}, & q' = q_{1_{--}}\\
p_{1_{+-}}^k(q) = \dfrac{(1-\alpha(q))\exp(\delta\xi_{1_{+-}}^k(q))}{C\,\mathrm{csh}(\delta\xi_{1_{+-}}^k(q))}, & q' = q_{1_{+-}}\\
p_{1_{-+}}^k(q) = \dfrac{(1-\alpha(q))\exp(-\delta\xi_{1_{+-}}^k(q))}{C\,\mathrm{csh}(\delta\xi_{1_{+-}}^k(q))}, & q' = q_{1_{-+}}\\
\vdots & \\
p_{(n/2)_{++}}^k(q) = \dfrac{(1+\alpha(q))\exp(\delta\xi_{(n/2)_{++}}^k(q))}{C\,\mathrm{csh}(\delta\xi_{(n/2)_{++}}^k(q))}, & q' = q_{(n/2)_{++}}\\
p_{(n/2)_{--}}^k(q) = \dfrac{(1+\alpha(q))\exp(-\delta\xi_{(n/2)_{++}}^k(q))}{C\,\mathrm{csh}(\delta\xi_{(n/2)_{++}}^k(q))}, & q' = q_{(n/2)_{--}}\\
p_{(n/2)_{+-}}^k(q) = \dfrac{(1-\alpha(q))\exp(\delta\xi_{(n/2)_{+-}}^k(q))}{C\,\mathrm{csh}(\delta\xi_{(n/2)_{+-}}^k(q))}, & q' = q_{(n/2)_{+-}}\\
p_{(n/2)_{-+}}^k(q) = \dfrac{(1-\alpha(q))\exp(-\delta\xi_{(n/2)_{+-}}^k(q))}{C\,\mathrm{csh}(\delta\xi_{(n/2)_{+-}}^k(q))}, & q' = q_{(n/2)_{-+}}\\
0, & \text{otherwise,}
\end{cases} \tag{24}
$$

where

$$
\xi_0^k(q) = \frac{4}{\lambda\bar{\sigma}^2} - 2n
$$

$$\xi^k_{i_{++}}(q) = \frac{[a(q,k\Delta t)]_i + [a(q,k\Delta t)]_{i+n/2}}{\eta_i \bar{\sigma}^2(1+\alpha(q))}, \quad i = 1,\ldots,n/2$$

$$\xi^k_{i_{+-}}(q) = \frac{[a(q,k\Delta t)]_i - [a(q,k\Delta t)]_{i+n/2}}{\eta_i \bar{\sigma}^2(1-\alpha(q))}, \quad i = 1,\ldots,n/2$$

$$C = \frac{4}{\lambda \bar{\sigma}^2}$$

λ is a positive constant that has to be chosen small enough such that $\xi^k_0(q)$ defined above is positive for all $q \in \mathcal{Q}$ and all $k \geq 0$. In particular, this is guaranteed if

$$0 < \lambda \leq (\bar{\sigma}^2 n/2)^{-1}. \tag{25}$$

The time elapsed between successive jumps is set equal to

$$\Delta t = \lambda \delta^2.$$

It can be verified that, with this choice for the neighboring set, the transition probabilities, and Δt, for each $q \in \mathcal{Q}^0$ and each $k \geq 0$,

$$m^k_q = \frac{2}{\lambda \delta C} \begin{bmatrix} \eta_1(1+\alpha(q))\dfrac{\mathrm{sh}(\delta \xi^k_{1_{++}}(q))}{\mathrm{csh}(\delta \xi^k_{1_{++}}(q))} + \eta_1(1-\alpha(q))\dfrac{\mathrm{sh}(\delta \xi^k_{1_{+-}}(q))}{\mathrm{csh}(\delta \xi^k_{1_{+-}}(q))} \\ \vdots \\ \eta_{n/2}(1+\alpha(q))\dfrac{\mathrm{sh}(\delta \xi^k_{(n/2)_{++}}(q))}{\mathrm{csh}(\delta \xi^k_{(n/2)_{++}}(q))} + \eta_{n/2}(1-\alpha(q))\dfrac{\mathrm{sh}(\delta \xi^k_{(n/2)_{+-}}(q))}{\mathrm{csh}(\delta \xi^k_{(n/2)_{+-}}(q))} \\ \eta_1(1+\alpha(q))\dfrac{\mathrm{sh}(\delta \xi^k_{1_{++}}(q))}{\mathrm{csh}(\delta \xi^k_{1_{++}}(q))} - \eta_1(1-\alpha(q))\dfrac{\mathrm{sh}(\delta \xi^k_{1_{+-}}(q))}{\mathrm{csh}(\delta \xi^k_{1_{+-}}(q))} \\ \vdots \\ \eta_{n/2}(1+\alpha(q))\dfrac{\mathrm{sh}(\delta \xi^k_{(n/2)_{++}}(q))}{\mathrm{csh}(\delta \xi^k_{(n/2)_{++}}(q))} - \eta_{n/2}(1-\alpha(q))\dfrac{\mathrm{sh}(\delta \xi^k_{(n/2)_{+-}}(q))}{\mathrm{csh}(\delta \xi^k_{(n/2)_{+-}}(q))} \end{bmatrix}$$

$$V^k_q = \begin{bmatrix} I & \alpha(q)I \\ \alpha(q)I & I \end{bmatrix} \Gamma^2$$

So if $\delta \to 0$ and we always choose q to be a point in $\mathcal{Q}^0$ closest to a fixed $s \in \mathcal{U} \setminus \mathcal{D}$, then

$$m^k_q \to a(s, k\Delta t)$$

$$V^k_q \to \begin{bmatrix} I & \alpha(q)I \\ \alpha(q)I & I \end{bmatrix} \Gamma^2 = b(s)\Gamma^2 b(s)^T.$$

Therefore, we conclude that Proposition 1 holds in this case as well.

Remark 3 *Note that one could analyze two aircraft encounters in the affine case without exploiting the information on the affine structure, and treating them as in the general case. However, the state Q of the resulting Markov chain would be of dimension 6 instead of 3, thus making the approximation procedure computationally much more expensive.*

3.3 An iterative algorithm for reachability computations

We next describe an iterative procedure to compute the probability $P_{c,\delta}$ that approximates the probability of conflict P_c in (17):

$$P_{c,\delta} \triangleq P\{Q_{k_f} \in \partial\mathcal{Q}_{\mathcal{D}}\} = P\{Q_k \text{ hits } \partial\mathcal{Q}_{\mathcal{D}} \text{ before hitting } \partial\mathcal{Q}_{\mathcal{U}} \text{ within } 0 \leq k \leq k_f\},$$

with the chain $\{Q_k, k \geq 0\}$ starting from a point $\bar{q} \in \mathcal{Q}$ closest to $S(0)$.
We address both the finite and infinite horizon cases ($k_f < \infty$ and $k_f = \infty$).

Let

$$P_{c,\delta}^{(k)}(q) \triangleq P\{Q_{k_f} \in \partial\mathcal{Q}_D |\, Q_k = q\}, \tag{26}$$

be a set of functions defined on $\mathcal{Q}$ and indexed by $k = 0, 1, \ldots, k_f$. Since the chain $\{Q_k, k \geq 0\}$ starts at $\bar{q}$ at $k = 0$, the desired quantity $P_{c,\delta}$ can be expressed in terms of the introduced functions as $P_{c,\delta}^{(0)}(\bar{q})$. The procedures described below determine the whole set of functions $P_{c,\delta}^{(k)} : \mathcal{Q} \to \mathbb{R}$ for $k = 0, 1, \ldots, k_f$. This has the advantage that at any future time $t \in [0, t_f]$ an estimate of the probability of conflict over the new time horizon $[t, t_f]$ is readily available, eliminating the need for re-computation. As a matter of fact, for each $t \in [0, t_f]$, $P_{c,\delta}^{(\lfloor t/\Delta t \rfloor)} : \mathcal{Q} \to \mathbb{R}$ represents an estimate of the probability of conflict over the time horizon $[t, t_f]$ as a function of the value taken by the state at time t.

To compute $P_{c,\delta}^{(0)}$, fix a k such that $0 \leq k < k_f$. It is easily seen then that $P_{c,\delta}^{(k)} : \mathcal{Q} \to \mathbb{R}$ satisfies the following recursive equation

$$P_{c,\delta}^{(k)}(q) = \begin{cases} p_q^k(q) P_{c,\delta}^{(k+1)}(q) + \sum_{q' \in \mathcal{N}_q} p_{q'}^k(q) P_{c,\delta}^{(k+1)}(q'), & q \in \mathcal{Q}^0 \\ 1, & q \in \partial\mathcal{Q}_{\mathcal{D}} \\ 0, & q \in \partial\mathcal{Q}_{\mathcal{U}}. \end{cases} \tag{27}$$

This is the key equation to compute $P_{c,\delta}^{(0)}$.

3.3.1 Finite horizon

In the finite horizon case ($k_f < \infty$), the probability $P_{c,\delta} = P_{c,\delta}^{(0)}(\bar{q})$ can be computed by iterating equation (27) backward k_f times starting from $k = k_f - 1$ and using the initialization $P_{c,\delta}^{(k_f)}(q) = \bar{P}(q)$, $q \in S$, where

$$\bar{P}(q) = \begin{cases} 1, & \text{if } q \in \partial S_D \\ 0, & \text{otherwise.} \end{cases} \tag{28}$$

The reason for the above initialization is obvious considering the definition (26) of $P_{c,\delta}^{(k)}$.

The procedure to compute an approximation of P_c in the finite horizon case is summarized in the following algorithm.

Algorithm 1 *Given* $S(0)$, $a : \mathbb{R}^n \times T \to \mathbb{R}^n$, $b : \mathbb{R}^n \to \mathbb{R}^{n \times n}$, Σ, *and* $\mathcal{D}$, *then*

1. *Select an open set* $\mathcal{U} \subset \mathbb{R}^n$ *containing* $\mathcal{D}$*, and fix* $\delta > 0$.

2. *Define the Markov chain* $\{Q_k, k \geq 0\}$ *with state space* $\mathcal{Q} = (\mathcal{U} \setminus \mathcal{D}) \cap \delta\mathbb{Z}^n$ *and appropriate transition probabilities.*

3. *Set* $\bar{k} = k_f$ *and initialize* $P_{c,\delta}^{(\bar{k})}$ *with* $\bar{P}$ *defined in equation (28).*

4. *For* $k = \bar{k} - 1, \ldots, 0$*, compute* $P_{c,\delta}^{(k)}$ *from* $P_{c,\delta}^{(k+1)}$ *according to equation (27).*

5. *Choose a point* $\bar{q}$ *in* S *closest to* $S(0)$ *and set* $P_{c,\delta} = P_{c,\delta}^{(0)}(\bar{q})$.

As for the choice of the grid size δ, one has to take into consideration different aspects:

i) In a time interval of length Δt, the maximal distance that the Markov chain can travel is $\eta_i \delta$ along the direction x_i, $i = 1, \ldots, n$. Thus given $\mathcal{U}$, for the diffusion process $S(t)$ to be approximated by the Markov chain, the component along the x_i axis $|[a(\cdot,\cdot)]_i|$ of $a(\cdot,\cdot)$ has to be upper bounded roughly by $\frac{\eta_i \delta}{\Delta t}$ over $T \times \mathcal{U} \setminus \mathcal{D}$, for any $i = 1, \ldots, n$. In view of Remark 2, this condition translates into upper bounds on the admissible values for δ. In particular, in the aircraft safety analysis case $\Delta t = \lambda \delta^2$, hence $\delta \leq \min_i \frac{\eta_i}{\lambda |[a(\cdot,\cdot)]_i|}$. Thus, fast diffusion processes cannot be simulated by Markov chains corresponding to large δ's.

ii) For a fixed grid size δ, the size of the state space $\mathcal{Q}$ is of the order of $1/\delta^n$, so each iteration in Algorithm 1 takes a time proportional to $1/\delta^n$. The number of iterations is given by $k_f \simeq t_f/\Delta t$. If Δt is proportional to δ^2 as in the safety analysis case, the running time of Algorithm 1 is proportional to $1/\delta^{n+2}$.

Therefore, for small δ's the running time may be too long, but large δ's may not allow for the simulation of fast moving processes. A suitable δ is a compromise between these two conflicting requirements.

Remark 4 *In aircraft-to-aircraft conflict detection, the size of the state space* $\mathcal{Q}$ *is of the order of* $1/\delta^3$ *in the affine case and* $1/\delta^6$ *in the general case. Due to the increase in the state space dimension, the running time of the Algorithm 1 applied to the general case is significantly larger than that of the same algorithm applied to the affine case. If the nonlinearity is relatively small, it might then be convenient to adopt a linear approximation so as to reduce the computational load.*

3.3.2 Infinite horizon

In the infinite horizon case $k_f = \infty$, hence Algorithm 1 cannot be applied directly since it would take infinitely many iterations. In this section we consider a special case in which this difficulty can be easily overcome.

We start by rewriting the iteration law (27) in matrix form. Arrange the sequence $\{P_{c,\delta}^{(k)}(q),\ q \in \mathcal{Q}^0\}$ into a long column vector according to some fixed ordering of the points in $\mathcal{Q}^0$, and denote

it by $\mathbf{P}_{c,\delta}^{(k)} \in \mathbb{R}^{|\mathcal{Q}^0|}$. Here $|\mathcal{Q}^0|$ is the cardinality of $\mathcal{Q}^0$. Then equation (27) can be written as

$$\mathbf{P}_{c,\delta}^{(k)} = \mathbf{A}^{(k)}\mathbf{P}_{c,\delta}^{(k+1)} + \mathbf{b}^{(k)} \tag{29}$$

for suitably chosen matrix $\mathbf{A}^{(k)} \in \mathbb{R}^{|\mathcal{Q}^0|\times|\mathcal{Q}^0|}$ and vector $\mathbf{b}^{(k)} \in \mathbb{R}^{|\mathcal{Q}^0|}$. Note that $\mathbf{A}^{(k)}$ is a sparse positive matrix with the property that the sum of its elements on each row is smaller than or equal to 1, where equality holds if and only if that row corresponds to a point in $(\mathcal{Q}^0)^0$, the interior of $\mathcal{Q}^0$ consisting of all those points in $\mathcal{Q}^0$ whose immediate neighbors all belong to $\mathcal{Q}^0$. On the other hand, $\mathbf{b}^{(k)}$ is a positive vector with nonzero elements on exactly those rows corresponding to points on the boundary $\partial(\mathcal{Q}^0) = \mathcal{Q}^0 \setminus (\mathcal{Q}^0)^0$ of $\mathcal{Q}^0$. Both $\mathbf{A}^{(k)}$ and $\mathbf{b}^{(k)}$ depend on the grid size δ. We do not write it explicitly to simplify the notation.

Suppose that from some time instant t_c on, $a(s,t)$ $s \in \mathbb{R}^n$, $t \in T$, remain constant in time, which makes sense in our aircraft conflict detection application since the ATC only has the aircraft flight plans and wind field information in the near future. Under this assumption, we have that $\mathbf{A}^{(k)} \equiv \mathbf{A}$ and $\mathbf{b}^{(k)} \equiv \mathbf{b}$ for $k > k_c \triangleq \lfloor \frac{t_c}{\Delta t} \rfloor$. Hence, for $k > k_c$ equation (29) becomes

$$\mathbf{P}_{c,\delta}^{(k)} = \mathbf{A}\mathbf{P}_{c,\delta}^{(k+1)} + \mathbf{b}. \tag{30}$$

We next address the problem of computing $\mathbf{P}_{c,\delta}^{(k_c+1)}$. Once we have determined $\mathbf{P}_{c,\delta}^{(k_c+1)}$, we can execute Algorithm 1 with step 2 replaced by

2'. Set $\bar{k} = k_c + 1$ and initialize $P_{c,\delta}^{(\bar{k})}$ with $P_{c,\delta}^{(k_c+1)}$.

to determine the approximation $P_{c,\delta}^{(0)}(\bar{q})$ of P_c.

The procedure to compute $\mathbf{P}_{c,\delta}^{(k_c+1)}$ rests on the following lemma.

Lemma 1 *The eigenvalues of* $\mathbf{A}$ *are all in the interior of the unit disk of the complex plane.*

Proof: Suppose that $\mathbf{A}$ has an eigenvalue γ with $|\gamma| \geq 1$, and let $\mathbf{v}$ be an eigenvector such that $\mathbf{A}\mathbf{v} = \gamma\mathbf{v}$. Assume that $|\mathbf{v}_i| = \max(|\mathbf{v}_1|, \ldots, |\mathbf{v}_{|\mathcal{Q}^0|}|)$ for some i. Then

$$|\mathbf{v}_i| \leq |\gamma\mathbf{v}_i| \leq |\,[\mathbf{A}\mathbf{v}]_i| \leq \sum_{j=1}^{|\mathcal{Q}^0|} \mathbf{A}_{ij}|\mathbf{v}_j| \leq \sum_{j=1}^{|\mathcal{Q}^0|} \mathbf{A}_{ij}|\mathbf{v}_i| \leq |\mathbf{v}_i|,$$

which is possible only if $|\mathbf{v}_1| = \cdots = |\mathbf{v}_{|\mathcal{Q}^0|}|$. However, this leads to a contradiction since by changing i in the above equation to one such that $\sum_{j=1}^{|\mathcal{Q}^0|} \mathbf{A}_{ij} < 1$, one gets $|\mathbf{v}_i| < |\mathbf{v}_i|$. ∎

Based on Lemma 1, we draw the following facts regarding equation (30):

Lemma 2 *Consider equation*

$$\mathbf{P}^{(k)} = \mathbf{A}\mathbf{P}^{(k+1)} + \mathbf{b}. \tag{31}$$

i) There is a unique $\mathbf{P} \in \mathbb{R}^{|\mathcal{Q}^0|}$ *satisfying*

$$\mathbf{P} = \mathbf{A}\mathbf{P} + \mathbf{b}. \tag{32}$$

ii) Starting from any initial value $\mathbf{P}^{(k_0)}$ *at some* k_0 *and iterating equation* (31) *backward in time,* $\mathbf{P}^{(k)}$ *converges to the fix point* $\mathbf{P}$ *as* $k \to -\infty$*. Moreover, if* $\mathbf{P}^{(k_0)} \geq \mathbf{P}$*, then* $\mathbf{P}^{(k)} \geq \mathbf{P}$ *for all* $k \leq k_0$*. Conversely, if* $\mathbf{P}^{(k_0)} \leq \mathbf{P}$*, then* $\mathbf{P}^{(k)} \leq \mathbf{P}$ *for all* $k \leq k_0$*. Note that here the symbols* $\geq$ *and* $\leq$ *denote component-wise comparison between vectors.*

Proof: $\mathbf{P} = (I - \mathbf{A})^{-1}\mathbf{b}$ since $I - \mathbf{A}$ is invertible by Lemma 1. Define $\mathbf{e}^{(k)} = \mathbf{P}^{(k)} - \mathbf{P}$. Then $\mathbf{e}^{(k)} = \mathbf{A}\mathbf{e}^{(k+1)}$. So by Lemma 1, $\mathbf{e}^{(k)}$ converges to 0 as $k \to -\infty$. The last conclusion is a direct consequence of the fact that all components of the matrix $\mathbf{A}$ and vector $\mathbf{b}$ are nonnegative. ■

Lemma 2 shows that equation (30) admits a fixed point $\mathbf{P}$ to which $\mathbf{P}^{(k)}$ obtained by iterating from any initial condition converges as $k \to -\infty$. Such a fixed point is in fact the desired quantity $\mathbf{P}_{c,\delta}^{(k_c+1)}$. Thus one way of computing $\mathbf{P}_{c,\delta}^{(k_c+1)}$ is to solve the linear equation $(I - \mathbf{A})\mathbf{P}_{c,\delta}^{(k_c+1)} = \mathbf{b}$ directly, using sparse matrix computation tools if possible. In our simulations, we determined $\mathbf{P}_{c,\delta}^{(k_c+1)}$ by iterating equation (31) starting at some k_0 from two initial conditions $\mathbf{P}_l^{(k_0)}$ and $\mathbf{P}_u^{(k_0)}$ that are respectively a lower bound and an upper bound of $\mathbf{P}$ (for example, one can choose $\mathbf{P}_l^{(k_0)}$ to be identically 0 on $\mathcal{Q}^0$ and $\mathbf{P}_u^{(k_0)}$ to be identically 1 on $\mathcal{Q}^0$). By Lemma 2, the iterated results at every $k \leq k_0$ for the two initial conditions will provide a lower bound and an upper bound of $\mathbf{P}_{c,\delta}^{(k_c+1)}$, respectively, which also converge toward each other (hence to $\mathbf{P}_{c,\delta}^{(k_c+1)}$ as well) as $k \to -\infty$. By running the iterations for the upper and lower bounds in parallel we can determine an approximation of $\mathbf{P}_{c,\delta}^{(k_c+1)}$ within any accuracy.

Remark 5 *As* $\delta \to 0$*, the size of the matrix* $\mathbf{A}$ *becomes larger. Moreover, the ratio* $|(\mathcal{Q}^0)^0|/|\mathcal{Q}^0| \to 1$*. Hence* $\mathbf{A}$ *will have an eigenvalue close to* 1 *whose corresponding eigenvector is close to* $(1, \ldots, 1)$*. This causes slower convergence for the iteration* (31) *and numerical problems for the solution to the fixed point equation* (32)*.*

3.4 Extension to the case when the initial state is uncertain

The procedure for estimating P_c can be easily extended to the case when the initial state $S(0)$ is not known precisely.

Suppose that $S(0)$ is described as a random variable with distribution $\mu_S(s)$, $s \in \mathcal{U} \setminus \mathcal{D}$. Then, the probability of entering the unsafe set $\mathcal{D}$ can be expressed as

$$P_c = \int_{\mathcal{U}\setminus\mathcal{D}} p_c(s) d\mu_S(s), \tag{33}$$

where $p_c : \mathcal{U} \setminus \mathcal{D} \to [0, 1]$ is defined by

$$p_c(s) \triangleq P\{S \text{ hits } \mathcal{D} \text{ before hitting } \mathcal{U}^c \text{ within the time interval } T \,|\, S(0) = s\}. \tag{34}$$

For each $s \in \mathcal{U} \setminus \mathcal{D}$, $p_c(s)$ is the probability of entering the unsafe set $\mathcal{D}$ over the time horizon T when $S(0) = s$ and is exactly the quantity estimated with $P_{c,\delta}^{(0)}$ in the iterative procedure proposed in Section 3.3. The integral (33) then reduces to a finite summation when approximating the map p_c with $P_{c,\delta}^{(0)}$.

4 Examples of probabilistic conflict detection in air traffic management

We present some examples where the proposed method for reachability analysis is applied to two problems arising in aircraft flight: the conflict between two aircraft, and the intrusion into a forbidden airspace area by a single aircraft.

In all the examples we adopt the iterative procedure described in Section 3.3 to estimate the probability of conflict during some look-ahead time horizon.

4.1 Two aircraft encounters: flight-level case

We consider two aircraft flying in the same region of the airspace at a fixed altitude. The two aircraft system is described by equations (3) and (4), with X_1 and X_2 denoting the two aircraft positions and taking values in $\mathbb{R}^2$. Note that the model described in Section 2 refers to the 3D flight case, where the aircraft positions take value in $\mathbb{R}^3$. However, it can be easily reformulated for the 2D case by minor modifications. In the 2D case, the unsafe set is a circle of radius r centered at the origin.

In the following examples the safe distance r is set equal to 3, whereas the spatial correlation function ρ and matrix Σ are given by $\rho(y) = \exp(-c\|y\|)$, $y \in \mathbb{R}^2$ and $\Sigma = \sigma I$, where c and σ are positive constants. In all the plots of the estimated probability of conflict, the reported level curves refer to values $0.1, 0.2, \ldots, 0.9$.

4.1.1 Affine case

Suppose that the wind field is affine in space and given by

$$f(x,t) = R(t)x + d(t),\ t \in T,\ x \in \mathbb{R}^2.$$

For the purpose of computing the probability of conflict, the two aircraft system can be described in terms of the aircraft relative position Y as follows:

$$dY(t) = v(t)dt + R(t)Y(t)dt + \sqrt{2[1-\rho(Y(t))]}\sigma\, dW(t), \tag{35}$$

where $W(\cdot)$ is a standard 2D Brownian motion, and $v : T \to \mathbb{R}^2$ is the aircraft relative velocity. A conflict occurs when Y enters the unsafe set $\mathcal{D} = \{y \in \mathbb{R}^2 : \|y\| \leq r\}$, where $r = 3$. Y can be approximated weakly by a Markov chain defined by the procedure described in Section 3.2.1 with the parameter λ appearing in (22) set equal to $\lambda = (4\sigma^2)^{-1}$.

Unless otherwise stated, in all of the examples in this subsection we use the following parameters:

The time interval of interest is $T = [0, 40]$. The relative velocity of the two aircraft during the time horizon T is given by

$$v(t) = \begin{cases} (2,0), & 0 \leq t < 10; \\ (0,1), & 10 \leq t < 20; \\ (2,0), & 20 \leq t \leq 40. \end{cases}$$

The parameter σ is equal to 1.
Based on the values of T and $v(t)$, $t \in T$, the domain $\mathcal{U}$ is chosen to be the open rectangle $(-80, 10) \times (-40, 10)$. The grid size is $\delta = 1$, hence the sampling time interval is $\Delta t = \lambda\delta^2 = (4\sigma^2)^{-1}\delta^2 = 0.25$.

Example 1 We consider the case when the wind field is identically zero: $f(x,t) = 0$, for all $t \in T$, $x \in \mathbb{R}^2$. We set $c = 0.2$ in the spatial correlation function ρ. In Figure 5 we plot the level curves of the estimated probability of conflict over the time horizon $[t, t_f]$ as a function of the aircraft relative position at time t. As one can expect, the probability of conflict over $[t, t_f]$ takes higher values along the nominal path, which is the path traced by a point that starts from the origin at time $t_f = 40$ and moves backward in time according to the nominal relative velocity $v(\cdot)$ until time t. Furthermore, as the relative positions between the aircraft at time t moves farther away from that path, the probability of conflict decreases. Experiments (not reported here) show that the smaller the variance parameter σ, the faster this decrease.

Example 2 This example differs from the previous one only in the value of c, which is now set equal to $c = 0.05$. Then $\rho(y) = \exp(-0.05\|y\|)$ for $y \in \mathbb{R}^2$, which decreases much more slowly than in the previous case as $\|y\|$ increases. Since ρ characterizes the strength of spatial correlation in the random field $B(\cdot,\cdot)$, this means that the random components of the wind contributions to the two aircraft velocities tend to be more correlated to each other than in Example 1. In Figure 6, we plot the level curves of the estimated probability of conflict over $[t, t_f]$ in the cases $t = 0$, $t = 10$, and $t = 20$. One can see that, compared to the plots in Figure 5, the regions with higher probability of conflict in Figure 6 are more concentrated along the nominal path, which is especially evident near the origin. In a sense, this implies that the current approaches to estimating the probability of conflict, based on the assumption of independent wind perturbations to the aircraft velocities, could be pessimistic. The intuitive explanation of this phenomenon is that random wind perturbations to the aircraft velocities with larger correlations are more likely to cancel each other, resulting in more predictable behaviors and hence smaller probability of conflict.

Example 3 In this example, we choose $c = 0.05$ as in Example 2. However, we assume that there is a nontrivial affine wind field f defined by

$$f(x,t) = R(t)[x - z(t)], \quad x \in \mathbb{R}^2,\ t \in [0, 40],$$

where

$$R(t) \equiv \frac{1}{50}\begin{bmatrix} 0 & 1 \\ -1 & 0 \end{bmatrix}, \quad z(t) = \begin{bmatrix} 3t \\ t^2/5 \end{bmatrix}.$$

The wind field f can be viewed as a windstorm swirling clockwise, whose center $z(t)$ accelerates along a curve during T. In fact, the choice of $z(t)$ will have no effect on the probability of conflict since it does not affect the aircraft relative position. In the first row of Figure 7, we plot the wind field f in the region $[-100, 200] \times [-100, 200]$ at the time instant $t = 0$ and the level curves of the estimated probability of conflict over $[t, t_f]$, at $t = 0$. In the second and third rows we represent similar plots for $t = 10$ and $t = 20$, respectively. One can see that, compared to the results in Figure 6, the regions with high probability of conflict are "bent" counterclockwise,

and the farther away from the origin, the more the bending. This is because the net effect of the wind field f on the relative velocity v of the two aircraft is RY, which points clockwise when the relative position Y is in the third quarter of the Cartesian plane.

Example 4 Suppose now that in Example 3 we change the ending epoch t_f from 40 to infinity, and assume that the relative velocity v remains constant and equal to $(2, 0)^T$ from time 20 on. For this infinite horizon problem, we can obtain an estimate of the probability of conflict at time $t = 0, 10, 20$ as drawn from top to bottom in Figure 8. Note that, unlike in the previous examples, the regions with high probability of conflict extend outside the domain $\mathcal{U}$ and are truncated. This is the price we pay to evaluate numerically the probability of conflict.

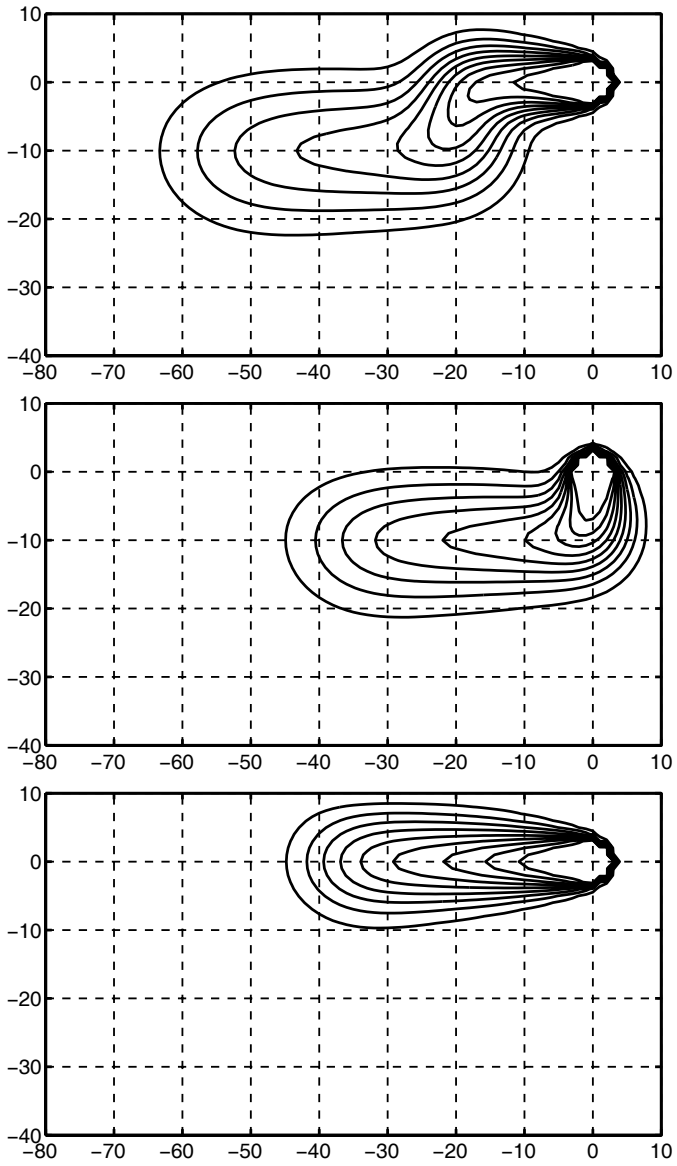

Figure 5: Example 1. Level curves of the estimated probability of conflict over the time horizon $[t, 40]$. Top: $t = 0$. Center: $t = 10$. Bottom: $t = 20$. ($c = 0.2$)

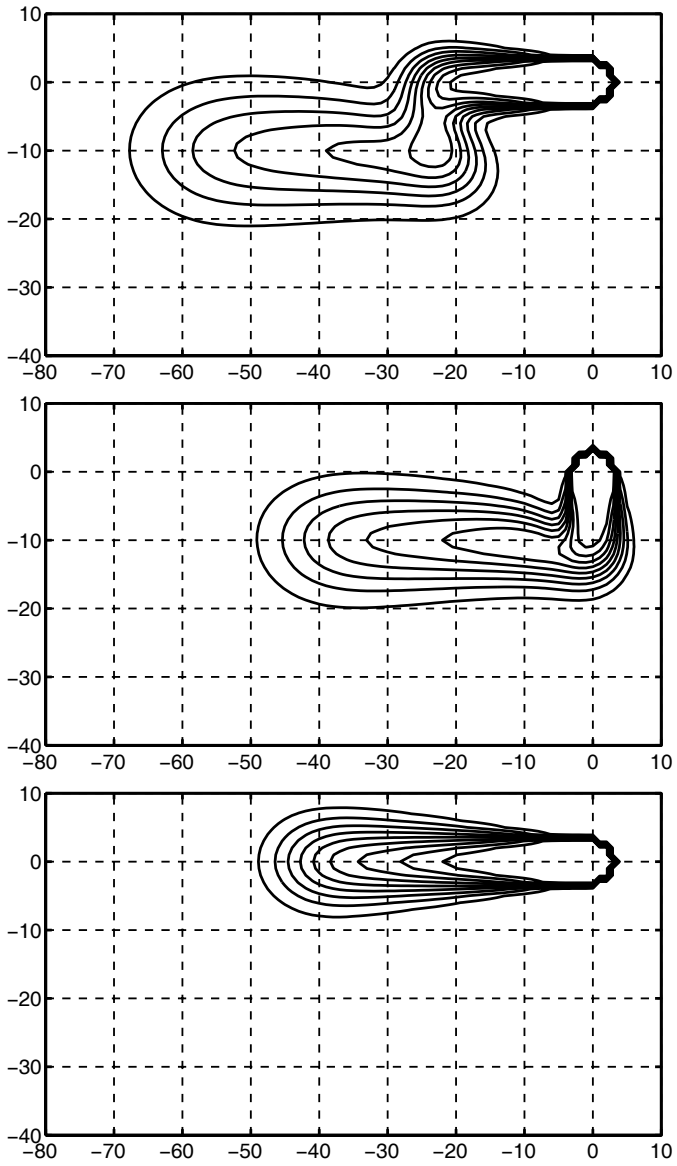

Figure 6: Example 2. Level curves of the estimated probability of conflict over the time horizon $[t, 40]$. Top: $t = 0$. Center: $t = 10$. Bottom: $t = 20$. ($c = 0.05$)

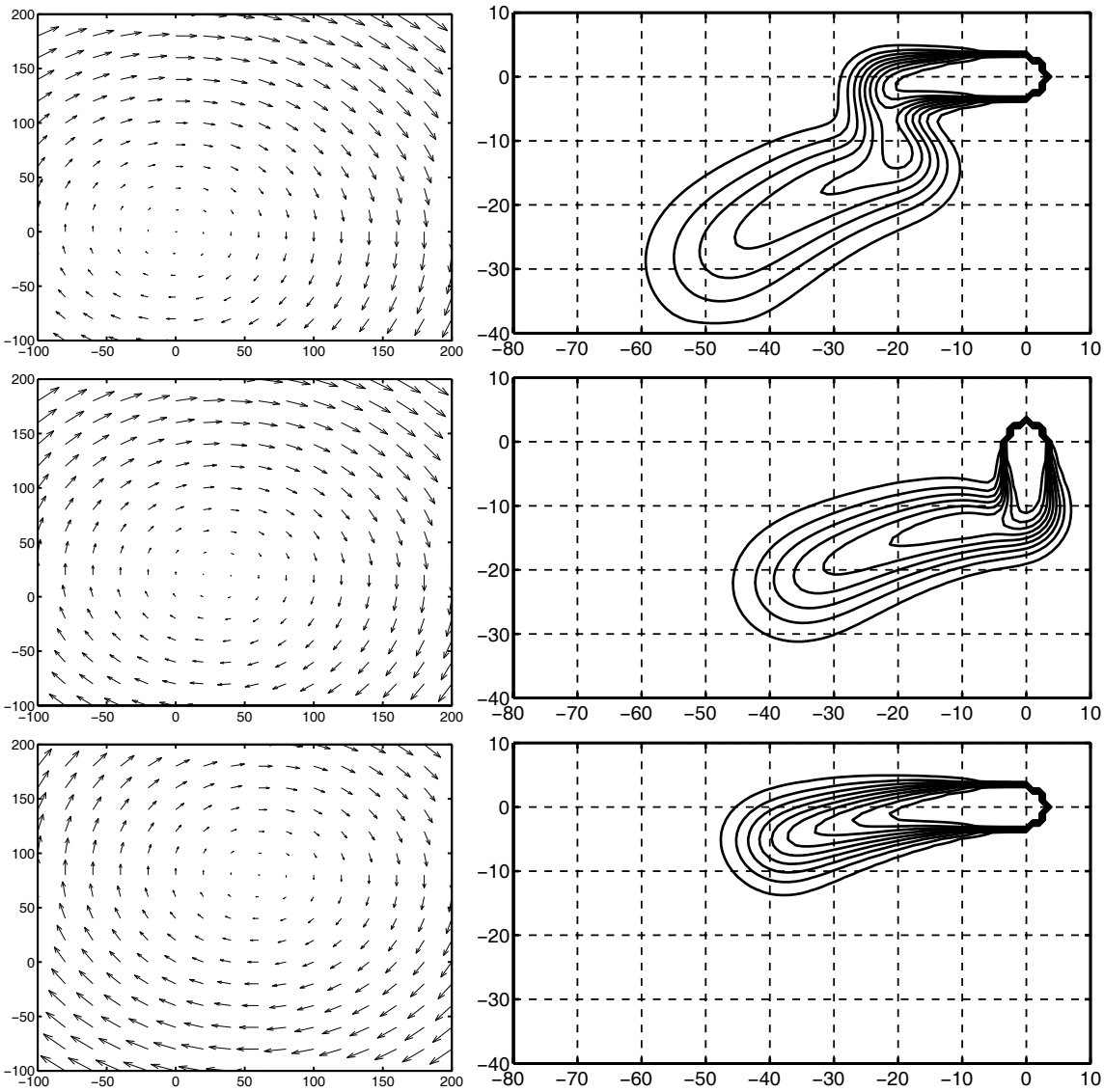

Figure 7: Example 3. Wind field at time t, and level curves of the estimated probability of conflict over the time horizon $[t, 40]$. Top: $t = 0$. Center: $t = 10$. Bottom: $t = 20$. ($c = 0.05$)

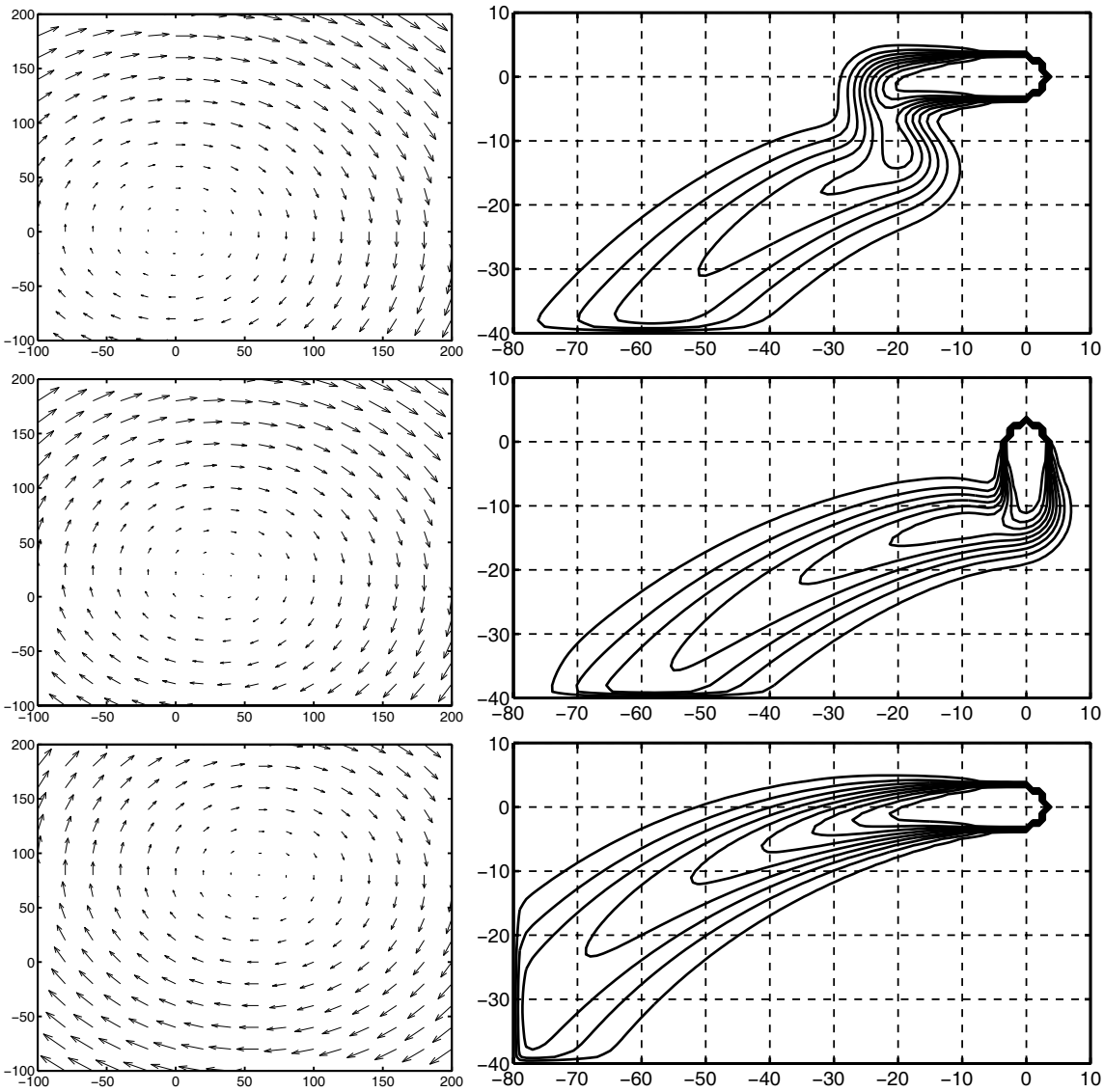

Figure 8: Example 4. Wind field at time t, and level curves of the estimated probability of conflict over the time horizon $[t, \infty]$. Top: $t = 0$. Center: $t = 10$. Bottom: $t = 20$. ($c = 0.05$)

4.1.2 General case

In the general wind field case (i.e. when the wind field is not necessarily affine in space), we have to keep track of the aircraft positions X_1 and X_2 for computing the probability of conflict. Let

$$\hat{X} = \begin{bmatrix} X_1 \\ X_2 \end{bmatrix} \in \mathbb{R}^4.$$

Then

$$d\hat{X}(t) = \hat{u}(t)dt + \hat{f}(\hat{X}(t), t)dt + \begin{bmatrix} I_2 & \hat{\rho}(\hat{X}(t))\, I_2 \\ \hat{\rho}(\hat{X}(t))\, I_2 & I_2 \end{bmatrix}^{1/2} \sigma d\hat{W}(t),$$

where $\hat{W}(t)$ is a standard Brownian motion in $\mathbb{R}^4$,

$$\hat{u}(t) = \begin{bmatrix} u_1(t) \\ u_2(t) \end{bmatrix}, \quad \hat{f}(\hat{X}, t) = \begin{bmatrix} f(X_1, t) \\ f(X_2, t) \end{bmatrix}, \quad t \in T$$

and $\hat{\rho}(\hat{X}) \triangleq \rho(X_2 - X_1)$.

$\hat{X}$ can be approximated weakly by a Markov chain defined by the procedure described in Section 3.2.2 with the parameter λ appearing in (24) set equal to $\lambda = (2\sigma^2)^{-1}$. In the case when the wind field is actually affine in space, experiments show that the results obtained based on this description of the two aircraft system are in agreement with those obtained based on description (35), with the disadvantage that in the former case computations are more intensive. Here we report only an example where the wind-field is non-affine.

Example 5 In this example, the time interval of interest is $T = [0, 20]$. The velocities of the two aircraft during the time horizon T are supposed to be constant and given by

$$u_1(t) = \begin{bmatrix} 4 \\ 0 \end{bmatrix}, \quad u_2(t) = \begin{bmatrix} 2 \\ 0 \end{bmatrix}, \quad 0 \le t \le 20.$$

The wind field is assumed to depend only on the spatial coordinate $x \in \mathbb{R}^2$ as follows

$$f(x, t) = \begin{bmatrix} \frac{\exp[([x]_1+20)/2]-1}{\exp[([x]_1+20)/2]+1} \\ 0 \end{bmatrix},$$

where $[x]_1$ is the first component of x. A plot of f is shown in Figure 9.

As for the stochastic component of the wind, we consider the case when $\sigma = 2$ and $c = 1$.

Based on the values taken by T, and $u_1(t), u_2(t)$, $t \in T$, we set $\mathcal{U} \triangleq \mathcal{U}_1 \times \mathcal{U}_2$, with $\mathcal{U}_1$ and $\mathcal{U}_2$ open rectangles $\mathcal{U}_1 = (-100, 30) \times (-24, 24)$ and $\mathcal{U}_2 = (-60, 80) \times (-16, 16)$. Finally, we set $\lambda = (2\sigma^2)^{-1} = 0.125$ and $\delta = 1.5$, so that $\Delta t = \lambda\delta^2 = 9/32$.

In Figure 10, we plot the level curves of the estimated probability of conflict as a function of the initial position of aircraft 1, for five different initial positions of aircraft 2: $(-40, 0)$, $(-30, 0)$,

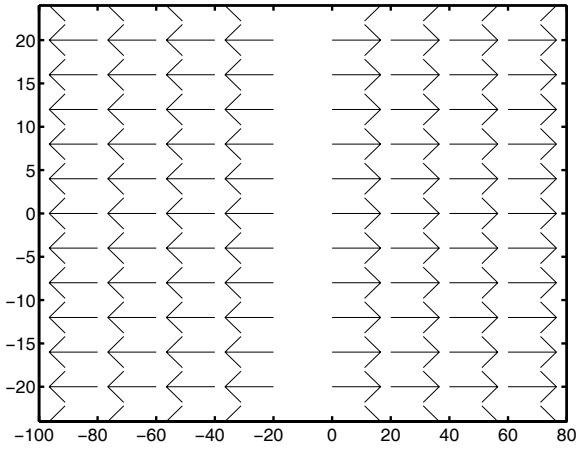

Figure 9: Example 5. Non-affine wind field.

$(-20, 0)$, $(0, 0)$, and $(20, 0)$, moving from top to bottom in the figure. On each row, the figure on the left side corresponds to the probability of conflict as computed by Algorithm 1. Since we use a relative coarse grid $\delta = 1.5$, the level curves are not smooth. For better visualization, we plot on the right side the level curves of a smoothed version of the probability of conflict maps, whose value at each grid point $w \in \mathcal{U}_1 \cap \delta\mathbb{Z}^2$ is the average value of the probability of conflict at w and its four immediate neighboring points w_{1-}, w_{1+}, w_{2-}, w_{2+}. In effect, this is equivalent to passing the original probability of conflict map through a low pass filter

$$\frac{1}{5}\begin{bmatrix} 0 & 1 & 0 \\ 1 & 1 & 1 \\ 0 & 1 & 0 \end{bmatrix}.$$

This also corresponds to assuming that there is uncertainty in the initial position of aircraft 1, such that it is equally probable that aircraft 1 occupies its nominal position and the four immediate neighboring grid points.

In the reported example, we see that, unlike the affine wind field case, the probability of conflict in general depends on the initial positions of both aircraft, not just on their initial relative position. If the probability of conflict would depend only on the aircraft initial relative position, then the level curves in the plots of Figure 10 will be all identically shaped and one could be obtained from another by translation of an amount given by the difference between the corresponding initial positions of aircraft 2, which is obviously not the case in Figure 10.

The dependence of the probability of conflict on the initial positions of both aircraft rather than simply their relative position is more eminent at those places where there is a large acceleration (or deceleration) in wind components, i.e., at those places with higher degree of nonlinearity in the wind field. If the nonlinearity of the wind field is relatively small, the two aircraft system could be described in terms of the their relative position (equation (35)), significantly reducing the computation time.

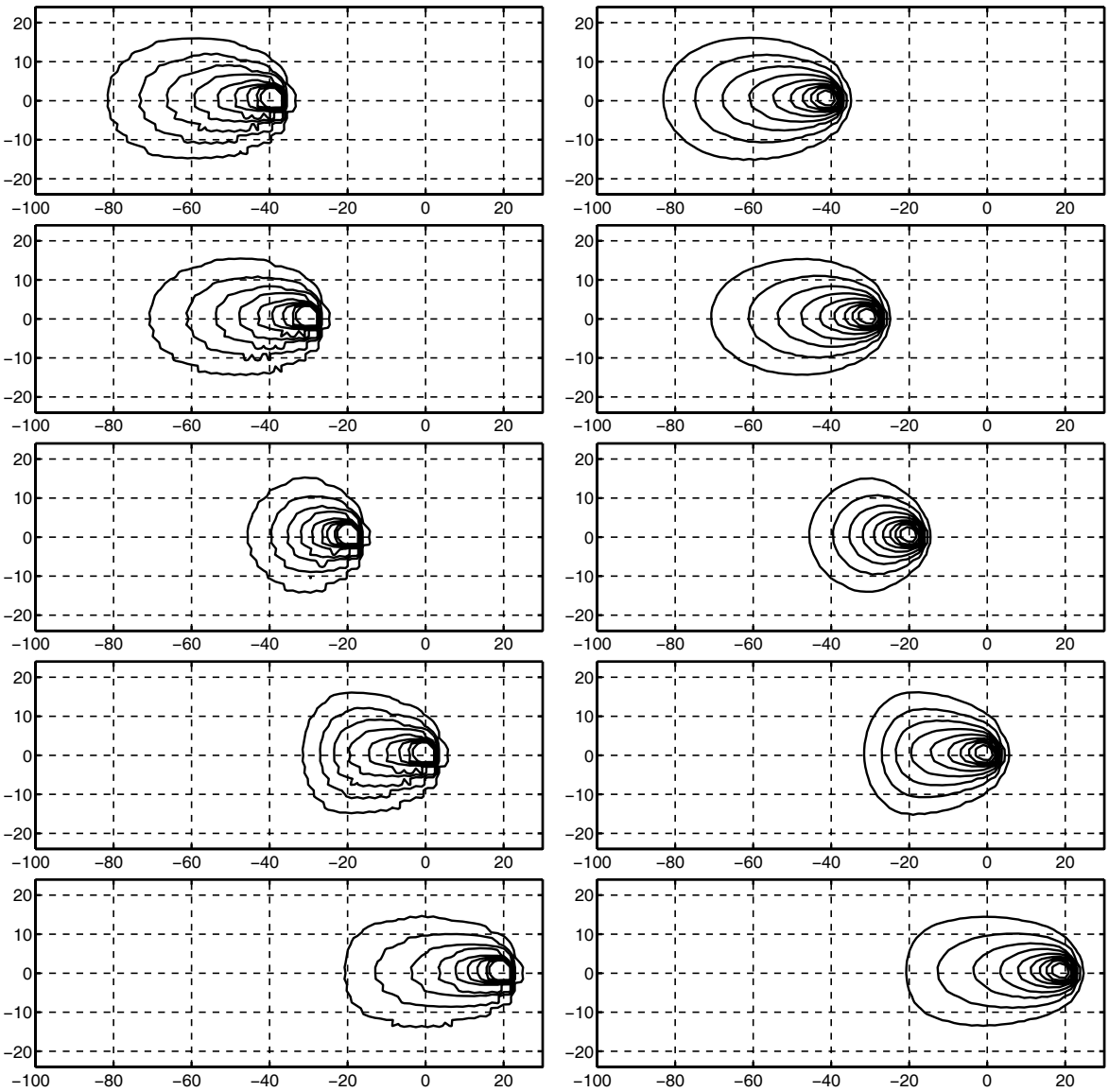

Figure 10: Example 5. Left: Level curves of the estimated probability of conflict over the time horizon $[0, 20]$ as a function of the initial position of aircraft 1 for fixed initial position of aircraft 2 (from top to bottom: $(-40, 0)$, $(-30, 0)$, $(-20, 0)$, $(0, 0)$, and $(20, 0)$). Right: Level curve of a smooth version of the corresponding quantity on the left (Non-affine wind field.)

4.2 Two aircraft encounters: three dimensional case

We consider a two aircraft encounter where the aircraft positions X_1 and X_2 take values in $\mathbb{R}^3$ and are governed by equations (3) and (4).

The wind field f is assumed to be identically zero, so that the probability of conflict can be computed by referring to the aircraft relative position Y:

$$dY(t) = v(t)dt + \sqrt{2[1-\rho(Y(t))]}\Sigma\, dW(t), \tag{36}$$

where $W(\cdot)$ is a standard 3D Brownian motion, and v is the aircraft relative velocity. A conflict occurs when Y enters the unsafe set $\mathcal{D} = \{y \in \mathbb{R}^2 : \|y\|_h \leq r,\ \|y\|_v \leq H\}$. Here we set $r = 3$ and $H = 1$.

We consider the case when $\rho(y) = \exp(-c_h\|y\|_h - c_v\|y\|_v)$, $y \in \mathbb{R}^3$, with c_h and c_v positive constants, and the matrix Σ is given by $\Sigma = \mathrm{diag}(\sigma_h, \sigma_h, \sigma_v)$, where $\sigma_h = 1$ and $\sigma_v = 0.5$.

We evaluate the probability that a conflict situation occurs within the time horizon $T = [0, 40]$, when the relative velocity of the two aircraft during T is given by

$$v(t) = \begin{cases} (2,0,0), & 0 \leq t < 5; \\ (0,1,1), & 5 \leq t \leq 10. \end{cases}$$

Based on the values taken by T, $v(\cdot)$, r and H, we choose the domain $\mathcal{U}$ to be $\mathcal{U} = (-30, 15) \times (-15, 10) \times (-15, 10)$. We set the discretization step size $\delta = 1$, and $\lambda = (6\sigma_h^2)^{-1} = 1/6$. Thus $\Delta t = \lambda\delta^2 = 1/6$.

Figure 11 represents the estimated probability of conflict over the time horizon $[0, 10]$ as a function of the relative position of the two aircraft at time t. The plots refer to the cases when $c_h = 0.2$, $c_v = 0.5$ and $c_h = 0.05$, $c_v = 0.05$ shown column-wise from left to right. In each column, we have the three dimensional isosurface at value 0.2 of the estimated probability of conflict viewed from different angles. The relevance of isosurfaces is that, in practice, once the relative position of the two aircraft is within the isosurface at a prescribed threshold value, an alarm of corresponding severity should be issued to the pilots to warn them on the level of criticality of the situation ([9]).

Note that when the parameters c_h and c_v of the spatial correlation function ρ are set equal to $c_h = c_v = 0.05$, the wind spatial correlation is increased. As a consequence of this fact, the isosurface at 0.2 concentrates more tightly along the deterministic path that leads to a conflict, and it extends longer as well.

4.3 Restricted areas in three dimensional airspace

Suppose that an aircraft is flying along the x_1-axis while climbing up at an accelerated rate according to the flight plan $u(t) = (3/2, 0, 2t/75)$, $t \in T = [0, 15]$, and that its motion is described by

$$dX(t) = u(t)dt + \Sigma\, dW(t),$$

where W is a standard 3-dimensional Brownian motion and $\Sigma = \mathrm{diag}(\sigma_h, \sigma_h, \sigma_v)$, where $\sigma_h = 1$ and $\sigma_v = 0.5$.

Consider a prohibited airspace area $\mathcal{D}$ given by the union of two ellipsoids: the first one specified by

$$\{(x_1, x_2, x_3) \in \mathbb{R}^3 : 2(x_1 + 4)^2 + (x_2 - 4)^2 + 10x_3^2 \leq 9\},$$

and the second one specified by

$$\{(x_1, x_2, x_3) \in \mathbb{R}^3 : x_1^2 + 2(x_2 + 5)^2 + 10x_3^2 \leq 16\},$$

in the (x_1, x_2, x_3) Cartesian coordinate system with x_3 representing the flight level.

Figure 12 shows the plots of the isosurface at value 0.2 of the probability of conflict as a function of the aircraft initial position, at time $t = 0$, $t = 5$, and $t = 10$, viewed from three different angles. The probability of conflict is estimated through Algorithm 1 with $\mathcal{U} = (-38, 6) \times (-15, 11) \times (-6, 3)$ and $\delta = 1$.

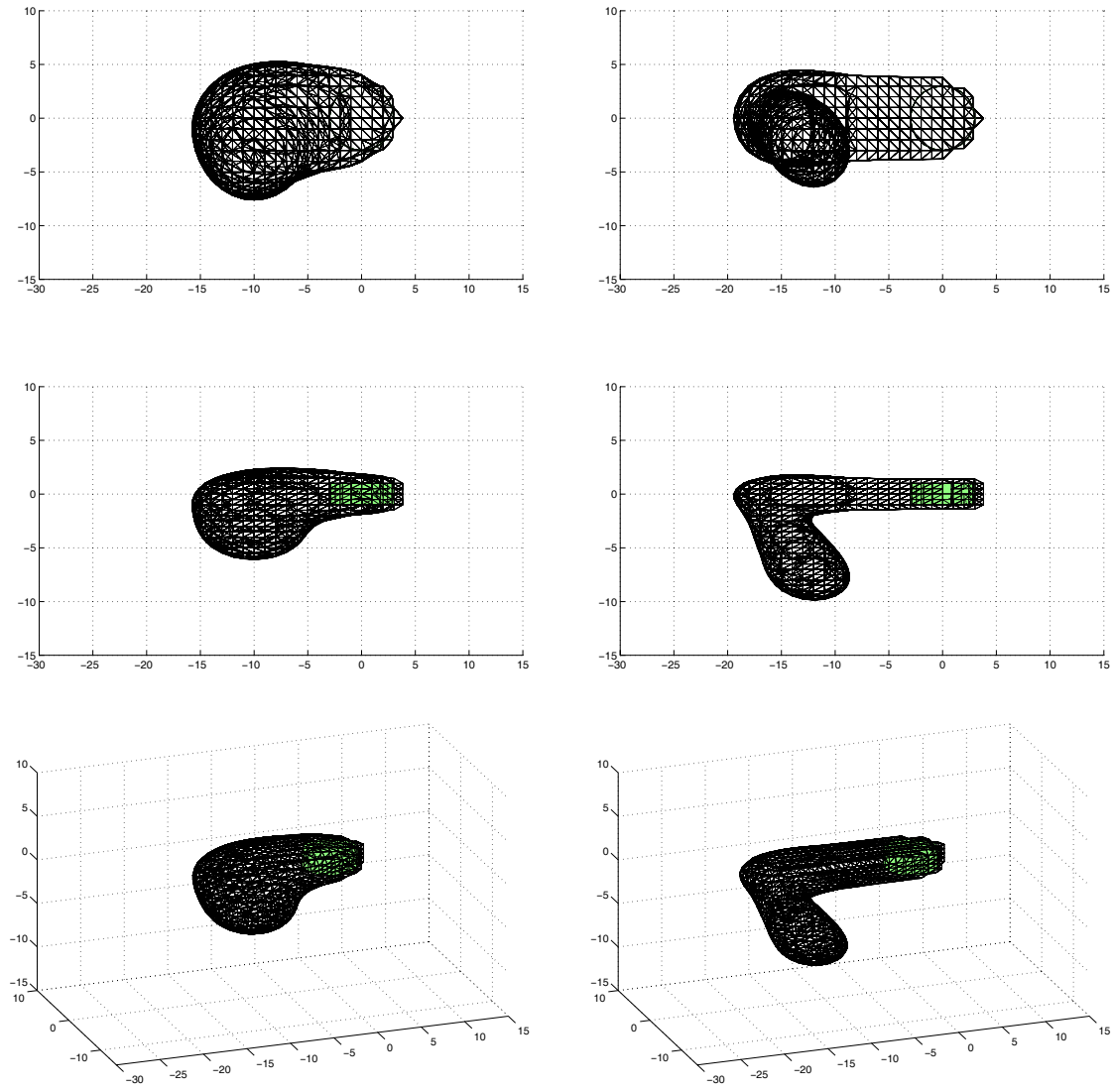

Figure 11: Estimated probability of conflict over the time horizon $[0, 10]$: isosurface at value 0.2. Left: $c_h = 0.2$ and $c_v = 0.5$. Right: $c_h = 0.05$ and $c_v = 0.05$. First row: top view. Second row: side view. Third row: three dimensional plot.

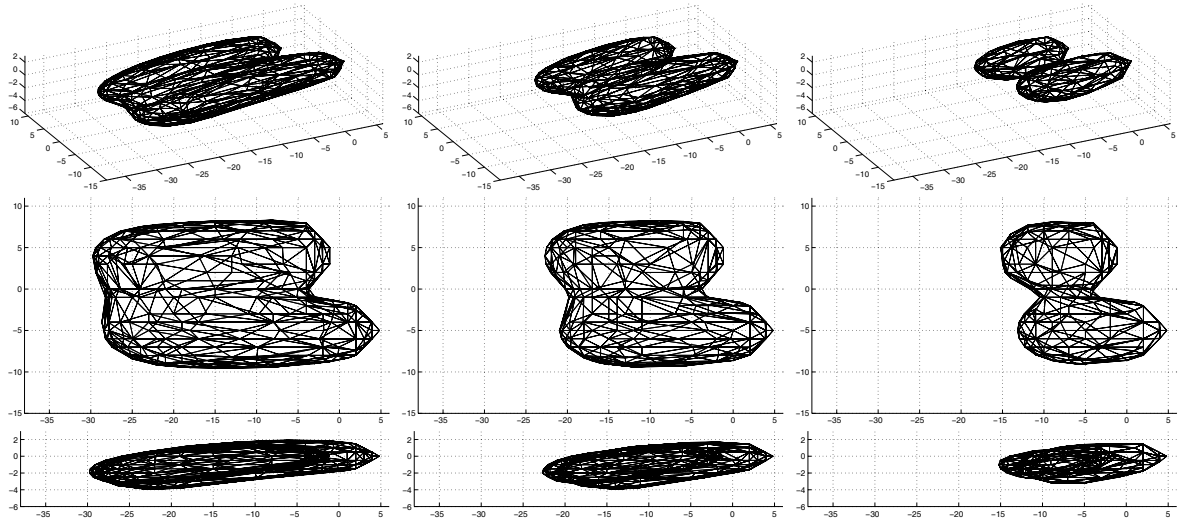

Figure 12: Estimated probability of conflict over the time horizon $[t, 15]$: isosurface at value 0.2. Left: $t = 0$. Center: $t = 5$. Right: $t = 10$. First row: 3D plot. Second row: top view. Third row: side view.

5 Conclusions

We developed a novel grid-based method for estimating the probability that two aircraft flying in the same region of the airspace get closer than a certain safety distance and the probability that an aircraft enters a forbidden airspace area. The intended application is aircraft conflict detection, with the final objective of supporting air traffic controllers in detecting potential conflict situations so as to improve the efficiency of the air traffic management system in terms of airspace usage.

A main feature of the proposed method is that the probability of conflict is evaluated based on a probabilistic model of the aircraft motion that takes into account the spatial correlation of wind. Specifically, a kinematic model of the aircraft motion in a three dimensional wind field with spatially correlated random perturbations is introduced. Based on this model, an iterative algorithm is proposed to estimate the probability of occurrence of a conflict event within some look-ahead time horizon given the aircraft flight plans. This algorithm is based on a Markov chain approximation scheme.

The model used to predict the aircraft future positions over the look-ahead time horizon is quite simple: the aircraft should follow a piecewise constant velocity profile, but its actual velocity is the sum of the nominal velocity and the wind speed. However, the proposed method for flight-plan-level conflict analysis can be extended to address more general cases. For example, the forbidden airspace area may evolve in time. Also, the model of the aircraft motion can be made more complicated, for example, including a corrective action of the flight management system on the aircraft velocity, a dependence on the altitude of the random field variance, or even considering a second order dynamics model with the wind affecting both first-order and second-order terms. In each of these cases, one can adopt the same approximation scheme. However, the dimension of the state space of the resulting Markov chain is generally larger than that of the case addressed in this work.

Grid-based methods are generally computationally intensive. On the other hand, the outcome of the proposed grid-based algorithm is a map that associates to each admissible aircraft position pairs the corresponding estimate of the probability of conflict, which could be used not only for conflict detection, but also for designing feedback control for conflict avoidance. One could, for example, force the aircraft to slide along a certain iso-surface, with the isosurface value depending on the trust level (manned or unmanned operation). Another possibility would be to choose as resolution maneuver a change of heading towards the direction of the negative gradient of the probability of conflict function, following the greedy approach proposed in [15], inspired by the potential field theory.

It is worth noticing that, though we concentrate on air traffic control, our results may have potentials in other safety-critical contexts. Aircraft conflict prediction is in fact a particular instance of the more general stochastic reachability analysis problem of evaluating if the trajectories of a given stochastic system will eventually enter an unsafe set.

6 Acknowledgments

The model for aircraft motion prediction described in this deliverable was inspired by some joint work with John Lygeros under workpackage 1 of the HYBRIDGE project ([29]).

The model and the algorithm for reachability computations have appeared in [25], [26], and [27], jointly written with Jianghai Hu and Shankar Sastry from the University of California at Berkeley.
The research on reachability analysis for air traffic management applications started in June 2002, while Jianghai Hu was visiting the University of Brescia for one month period, supported by the HYBRIDGE funding.

References

[1] C. Tomlin, I. Mitchell, A. Bayen, and M. Oishi. Computational techniques for the verification and control of hybrid systems. *Proceedings of the IEEE*, 91(7):986–1001, 2003.

[2] R. Alur, T. Henzinger, G. Lafferriere, and G.J. Pappas. Discrete abstractions of hybrid systems. *Proceedings of the IEEE*, 88(2):971–984, 2000.

[3] A. Chutinan and B.H. Krogh. Verification of infinite-state dynamic systems using approximate quotient transition systems. *IEEE Transactions on Automatic Control*, 46(9):1401–1410, 2001.

[4] A.B. Kurzhanski and P. Varaiya. Ellipsoidal techniques for reachability analysis. In B. Krogh and N. Lynch, editors, *Hybrid Systems: Computation and Control*, Lecture Notes in Computer Science, pages 202–214. Springer Verlag, 2000.

[5] I. Mitchell and C. Tomlin. Level set methods for computation in hybrid systems. In B. Krogh and N. Lynch, editors, *Hybrid Systems: Computation and Control*, Lecture Notes in Computer Science, pages 310–323. Springer Verlag, 2000.

[6] I. Mitchell, A. Bayen, and C. Tomlin. Validating a Hamilton-Jacobi approximation to hybrid system reachable sets. In A. Sangiovanni-Vincentelli and M. Di Benedetto, editors, *Hybrid Systems: Computation and Control*, Lecture Notes in Computer Science, pages 418–432. Springer Verlag, 2001.

[7] J. Schrder and J. Lunze. Representation of quantised systems by the Frobenius-Perron operator. In A. Sangiovanni-Vincentelli and M. Di Benedetto, editors, *Hybrid Systems: Computation and Control*, Lecture Notes in Computer Science, pages 473–486. Springer Verlag, 2001.

[8] A.B. Kurzhanski and P. Varaiya. On reachability under uncertainty. *SIAM J. Control Optim.*, 41(1):181–216, 2002.

[9] L.C. Yang and J. Kuchar. Prototype conflict alerting system for free fligh. In *Proc. of the AIAA 35th Aerospace Sciences Meeting, AIAA-97-0220*, Reno, NV, January 1997.

[10] O. Watkins and J. Lygeros. Safety relevant operational cases in air traffic management, November 2002. HYBRIDGE Project IST-2001-32460, Work Package WP1, Deliverable D1.1.

[11] D.V. Dimarogonas and K.J. Kyriakopoulos. Inventory of decentralized conflict detection and resolution systems in air traffic, 2003. HYBRIDGE Project IST-2001-32460, Work Package WP6, Deliverable D6.1.

[12] Radio Technical Commission for Aeronautics. Minimum operational performance standards for traffic alert and collision avoidance system (TCAS) airborn equipment. Technical Report RTCA/DO-185, RTCA, September 1990. Consolidated Edition.

[13] J.K. Kuchar and L.C. Yang. A review of conflict detection and resolution modeling methods. *IEEE Transactions on Intelligent Transportation Systems, Special Issue on Air Traffic Control - Part I*, 1(4):179–189, 2000.

[14] R.A. Paielli and H. Erzberger. Conflict probability estimation for free flight. *Journal of Guidance, Control, and Dynamics*, 20(3):588–596, 1997.

[15] M. Prandini, J. Hu, J. Lygeros, and S. Sastry. A probabilistic approach to aircraft conflict detection. *IEEE Transactions on Intelligent Transportation Systems, Special Issue on Air Traffic Control - Part I*, 1(4):199–220, 2000.

[16] H. Erzberger, R.A. Paielli, D.R. Isaacson, and M.M. Eshow. Conflict detection and resolution in the presence of prediction error. In *Proc. of the 1st USA/Europe Air Traffic Management R & D Seminar*, Saclay, France, June 1997.

[17] J. Hu, M. Prandini, and S. Sastry. Optimal coordinated maneuvers for three dimensional aircraft conflict resolution. *Journal of Guidance, Control and Dynamics*, 25(5):888–900, 2002.

[18] C. Tomlin, G.J. Pappas, and S. Sastry. Conflict resolution for air traffic management: A study in multi-agent hybrid systems. *IEEE Transactions on Automatic Control*, 43(4):509–521, 1998.

[19] F. Medioni, N. Durand, and J.M. Alliot. Air traffic conflict resolution by genetic algorithms. In *Proc. of the Artificial Evolution, European Conference (AE 95)*, pages 370–383, Brest, France, September 1995.

[20] J. Hu, M. Prandini, and S. Sastry. Optimal maneuver for multiple aircraft conflict resolution: a braid point of view. In *Proc. of the* 39^{th} *Conf. on Decision and Control*, pages 4164–4169, Sydney, Australia, December 2000.

[21] J. Krozel and M. Peters. Strategic conflict detection and resolution for free flight. In *Proc. of the* 36^{th} *Conf. on Decision and Control*, volume 2, pages 1822–1828, San Diego, CA, December 1997.

[22] P.K. Menon, G.D. Sweriduk, and B. Sridhar. Optimal strategies for free-flight air traffic conflict resolution. *Journal of Guidance, Control, and Dynamics*, 22(2):202–211, 1999.

[23] Y. Zhao and R. Schultz. Deterministic resolution of two aircraft conflict in free flight. In *Proc. of the AIAA Guidance, Navigation, and Control Conference, AIAA-97-3547*, New Orleans, LA, August 1997.

[24] J. Kosecka, C. Tomlin, G.J. Pappas, and S. Sastry. Generation of Conflict Resolution Maneuvers For Air Traffic Management. In *Proc. of the IEEE Conference on Intelligent Robotics and System '97*, volume 3, pages 1598–1603, Grenoble, France, September 1997.

[25] J. Hu and M. Prandini. Aircraft conflict detection: a method for computing the probability of conflict based on Markov chain approximation. In *European Control Conf.*, Cambridge, UK, September 2003.

[26] J. Hu, M. Prandini, and S. Sastry. Optimal maneuver for multiple aircraft conflict resolution: a braid point of view. In *AIAA Guidance, Navigation, and Control Conference and Exhibit*, Austin, USA, August 2003.

[27] J. Hu, M. Prandini, and S. Sastry. Probabilistic safety analysis in three dimensional aircraft flight. In *Proc. of the* 42^{nd} *Conf. on Decision and Control*, Maui, USA, December 2003.

[28] J. Hu, J. Lygeros, M. Prandini, and S. Sastry. Aircraft conflict prediction and resolution using Brownian Motion. In *Proc. of the* 38^{th} *Conf. on Decision and Control*, Phoenix, AZ, December 1999.

[29] J. Lygeros and M. Prandini. Aircraft and weather models for probabilistic conflict detection. In *Proc. of the* 41^{st} *Conf. on Decision and Control*, Las Vegas, NV, December 2002.

[30] J. Lygeros and N. Lynch. On the formal verification of the TCAS conflict resolution algorithms. In *Proc. of the* 36^{th} *Conf. on Decision and Control*, pages 1829–1834, San Diego, CA, December 1997.

[31] R.J. Adler. *The Geometry of Random Fields.* John Wiley & Sons, 1981.

[32] E. H. Isaaks and R.M. Srivastava. *An Introduction to Applied Geostatistics.* Oxford University Press, 1989.

[33] R.E. Cole, C. Richard, S. Kim, and D. Bailey. An assessment of the 60 km rapid update cycle (RUC) with near real-time aircraft reports. Technical Report NASA/A-1, MIT Lincoln Laboratory, Jul. 1998.

[34] S. G. Benjamin, K. J. Brundage, P. A. Miller, T. L. Smith, G. A. Grell, D. Kim, J. M. Brown, T. W. Schlatter, and L. L. Morone. The Rapid Update Cycle at NMC. In *Proc. Tenth Conference on Numerical Weather Prediction*, pages 566–568, Portland, OR, Jul. 1994.

[35] R. Durrett. *Stochastic calculus: A practical introduction.* CRC Press, 1996.

[36] D.W. Stroock and S.R.S. Varadhan. *Multidimensional Diffusion Processes.* Springer-Verlag, 1979.